Theory of the magnetothermal instability in coronal plasma flows

F. García-Rubio[1,2,*], R. Betti[1,2,3], J. Sanz[4], and H. Aluie[1,2]
[1] *Laboratory for Laser Energetics, University of Rochester, 250 East River Road, Rochester, New York 14623-1299*
[2] *Department of Mechanical Engineering, University of Rochester, Rochester, New York 14627*
[3] *Department of Physics and Astronomy, University of Rochester, Rochester, New York 14627*
[4] *Escuela Técnica Superior de Ingeniería Aeronáutica y del Espacio, Universidad Politécnica de Madrid, Madrid 28040, Spain and*
[*] *Corresponding author: fgar@lle.rochester.edu*

The theory of the magnetothermal instability (MTI) [D. A. Tidman, and R. A. Shanny, Phys. Fluids **17**, 6 (1974)] is revisited through the lens of the stability of uniform systems. The linear stability analysis includes flow advection and Nernst transport. The instability criteria derived distinguish between the convective and the absolute nature of the perturbation growth. It is proven that, in the region where the Nernst and plasma blowoff velocities cancel, the MTI can be absolute and wave-packet perturbations grow *in situ*. This instability is mediated by the internal feedback between the Biermann-battery and Righi–Leduc terms. The analysis is extended to derive the dispersion relation for short-wavelength perturbations developing in nonuniform profiles with application to coronal plasmas. It is found that the condition for MTI requires the net B-field convection velocity to be small at the isothermal sonic section, and the plasma conditions in this section govern the dynamics of the instability. Analysis of hydro-equivalent implosions suggests that unstable perturbations undergo more e-foldings of growth in larger-size targets.

I. INTRODUCTION

It has long been known that self-generated magnetic (B) fields develop in laser-produced plasmas [1–4] and more recently in inertial confinement fusion (ICF) applications [5–7]. In the proton radiographies of ICF implosions obtained by Rygg *et al.* [5], complex filamentary B-field structures of magnitude ∼60 tesla were observed in the entire field of view of the corona. These electromagnetic fields can play an important role in ICF implosions because they modify heat transfer to the target and seed hydrodynamic instabilities, thereby degrading implosion performance.

Among the different sources leading to spontaneous B-field generation in laser-driven targets [8], the so-called Biermann-battery effect [9], which is due to misalignment between gradients of temperature and density, plays a dominant role in the conduction layer separating the ablation front from the coronal plasma past the critical surface. Activation of the Biermann-battery term requires certain flow complexity, as found in the hydrodynamic instabilities that develop in laser-produced plasmas. Experimental evidence of magnetic-field generation in ablation fronts undergoing ablative Rayleigh–Taylor instability (aRTI) has been reported by Manuel *et al.* [10] and Gao *et al.* [11, 12]. Its effect on the dynamics of the aRTI and the Darrieus–Landau instability (DLI) has been recently analyzed by García-Rubio *et al.* [13, 14], who found the B field to be stabilizing in the weak acceleration regime relevant to ICF.

The thermal conduction variation within the conduction zone in a coronal plasma leads to a disparity of length scales between the ablation front and the critical surface. This gives rise to the development of instabilities with different growth rates and dynamics. The instabilities previously discussed, of a hydrodynamic nature, present time scales given by the plasma conditions at the ablation front. However, the self-generated B field can trigger another instability on its own in the light, hot plasma of the corona. This instability, known as magnetothermal instability (MTI), was first described in the seminal papers by Tidman and Shanny [15] and Bol'shov *et al.* [16]. Unlike the aRTI, the MTI is not driven by an external acceleration. The underlying mechanism corresponds exclusively to the interplay between the Biermann battery generating B fields and the Righi–Leduc term bending the heat flux lines, as sketched in Fig. 1. In its most simple configuration, a temperature perturbation δT results in B-field generation $\delta\vec{B}$ via the Biermann battery. This allows the Righi–Leduc heat flux, $\vec{q}_{\rm RL} \propto \frac{T_0^4}{n_0}\nabla T_0 \times \delta\vec{B}$, to pump heat into the hotter regions of the fluid, therefore driving the MTI by amplifying the δT perturbation. The MTI is not the only instability related to B-field growth in laser-produced plasmas. Weibel-like instabilities [17, 18] and the electrothermal instability [19] can also develop in the corona. Amongst these different mechanisms, Séguin *et al.* [6] and Manuel *et al.* [7] were able to identify the MTI as the most likely mechanism explaining the filamentary fields observed in their proton radiographs of different configurations of laser-driven targets.

The seminal papers [15, 16] derived a condition for the MTI to develop in the limit of short perturbation wavelength. The condition required the base temperature and density gradients to be parallel, which implies that the MTI could only take place in the underdense plasma downstream of the critical surface. In the following years, the analysis was refined by taking into account plasma hydrodynamics and Nernst convection (B-field advection by electron heat flux), Refs. [20–22]. The criteria derived therein included regions with opposite gradients of tem-

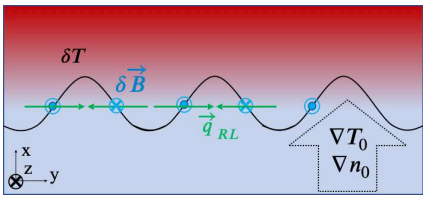

Figure 1. Schematic of the magnetothermal instability as first explained in Ref. [15]. It relied on the background ∇T_0 and ∇n_0 being aligned.

perature and density as potentially MTI unstable. Particularly, Dolginov and Urpin [20], who included Nernst but disregarded the plasma base flow, claimed the instability to be of a convective nature, that is, the perturbation grows while it propagates toward regions of lower temperature, i.e., ablation front and far corona.

These early-years analyses considered an unmagnetized base plasma. The effects of a background magnetization were explored by Fruchtman and Strauss [23] and, more recently, in the complete analysis of Bissell *et al.* [24, 25]. In the latter, the authors identified a secondary driving mechanism of the MTI arising from the interplay between B-field compression due to inhomogeneous Nernst convection and the Righi–Leduc heat flux. The authors contrasted this source with the Biermann-battery field-generating mechanism in the context of a low-density plasma in the nanosecond gas-jet experiment by Froula *et al.* [26]. They found the former to be the primary instability mechanism when the electron Hall parameter exceeded 0.1.

All the aforementioned analyses fall within the framework of uniform media and shed important light on the evolution of single-mode perturbations in the linear regime. In reality, however, initial perturbations come in a form of wave-packet with finite extent in space, and its evolution requires to distinguish between *convective* and *absolute* instability. In unstable systems, the packet spreads out and moves in space while its amplitude increases. If the perturbation moves sufficiently quickly that its amplitude tends asymptotically to zero at any fixed point, the instability is convective. If, however, the perturbation grows without limit at every point in space, the instability is absolute. It might appear that this difference is relative and depends on the frame of reference of choice. However, as noted in Landau and Lifshitz [27], "there is always an experimentally preferred frame of reference relative to which the instability is to be considered". For example, in an ICF target a perturbation can be convectively unstable and grows but is convected away from the target sufficiently fast such that it has little impact on the primary physical system of interest (the target). In contrast, an absolute instability in the frame of reference of the imploding shell can have a significant effect on its evolution.

There is extensive literature concerning the stability of uniform systems with application to plasma physics [28–32]. In the complete work of Briggs [30], criteria to distinguish between convective and absolute instability is provided based upon the analysis of the roots (modes) of the dispersion relation in Fourier space. In addition, Briggs highlights the physical difference between convectively and absolutely unstable systems. Convective instability is related to the ability of a system to support unstable waves, hence it needs of an external source to excite the system, whereas absolute instability is related to a spatial resonance inherent to the system. Establishing this difference is important in the context of the MTI. For example, Sherlock and Bissell [34] recently reported that the Nernst convection significantly reduced the growth rate in simulations of hohlraum-like plasmas because it advected the magnetic field from the corona, where it was generated.

In this paper, we extend the analysis of the MTI by applying the criteria given by Briggs [30] to discuss conditions under which this instability is absolute with relevance to coronal plasma flows. This paper is organized as follows. In Sec. II, the criterion for convective and absolute instability as derived in Briggs [30] is provided. A more rigorous review is given in App. A, where the relation to the stability of nonuniform profiles to short-wavelength perturbations is discussed. In Sec. III, the governing equations for a coronal plasma are presented and linearized. In Sec. IV, the conditions for convective and absolute MTI are derived. In Sec. V, the occurrence of the MTI in direct-drive implosions is discussed. Finally, in Sec. VI, conclusions are drawn.

II. CRITERION FOR CONVECTIVE AND ABSOLUTE INSTABILITY

We consider the evolution of a uniform, time-invariant, one-dimensional linear system with Green's function $G(t-\tau, x-\eta)$. Taking the Fourier and Laplace transformations as defined in Eqs. (A.2) and (A.3), respectively, and denoting $D(\omega,k) \equiv 1/G(\omega,k)$, with $G(\omega,k)$ being the transform of the Green's function, the dispersion relation of such system corresponds to the relation

$$D(\omega,k) = 0. \tag{1}$$

As thoroughly explained in Briggs [30], this expression contains all the information of the (linear) stabil-

ity of the system. In particular, it yields the unstable waves supported by the system, that is, the poles $\omega(k) : D(\omega, k) = 0$ satisfying $\mathrm{Im}[\omega(k)] < 0$ for a given real k. A system is *convectively unstable* if it supports unstable waves. In convectively unstable systems, the temporal behavior of the system is given by the frequency of the external excitation perturbing the system. The system amplifies such perturbation while being convected away from the source.

In contrast, absolute instability is related to a spatial resonance inherent to the system systems and, consequently, the temporal growth rate is intrinsic to the system and independent of the source. To obtain the criterion for absolute instability, it is more useful to consider the roots $k(\omega) : D(\omega, k) = 0$. Briggs based the absolute instability criterion on the translation of such roots in the Fourier space when the frequency ω changes. A system is *absolutely unstable* if the dispersion relation Eq. (1) yields two roots in the Fourier space coming from different halves of the complex k plane (upper and lower) that merge into one root for a frequency ω_s with $\mathrm{Im}(\omega_s) < 0$. Notice that absolutely unstable systems satisfy the convective instability criterion by definition, hence they also support unstable waves.

III. GOVERNING EQUATIONS

We apply the criteria derived in the previous section to obtain the growth rate of the magnetothermal instability to short-wavelength perturbations. We consider a plasma expanding due to laser energy deposition at a certain critical electron density n_c, and we denote T_c the characteristic electron temperature. We use a hydrodynamic description of a fully ionized, single-species plasma and we assume quasi-neutrality. We assume an atomic number Z large enough that the ion pressure can be neglected while the energy flow is still dominated by electronic heat conduction, and the ion energy equation is decoupled. The evolution of the electron density n, ion velocity $\vec{v}$, electron pressure p, electron temperature T, and magnetic-field intensity $\vec{B}$ are given by the electron continuity, total momentum, and total energy conservation together with Faraday's law of induction,

$$\frac{\partial n}{\partial t} + \nabla \cdot (n\vec{v}) = 0, \tag{2}$$

$$\bar{m} n \frac{\partial \vec{v}}{\partial t} + \bar{m} n \vec{v} \cdot \nabla \vec{v} = -\nabla p + \frac{1}{c}\vec{j} \times \vec{B}, \tag{3}$$

$$\frac{3}{2}\frac{\partial p}{\partial t} + \frac{3}{2}\nabla \cdot (p\vec{v}) + p\nabla \cdot \vec{v} = - \nabla \cdot \left(\vec{q}_e + \frac{5}{2}\vec{u}p\right) + \vec{u} \cdot \nabla p - \vec{R} \cdot \vec{u}, \tag{4}$$

$$\frac{\partial \vec{B}}{\partial t} + c\nabla \times \vec{E} = \vec{0}, \tag{5}$$

where $\bar{m}$ is the ion mass divided by the plasma atomic number, $\vec{E}$ is the electric field, and $\vec{j} = -en\vec{u}$ is the current, with $\vec{u}$ being the difference between electron and ion velocities. We have neglected the ion heat flux in Eq. (4) and electron inertia, and we use the ideal gas equation of state $p = nT$. The electric field and the current are given by the electron momentum conservation, which stands for a generalized Ohm's law and the Ampère's law, respectively,

$$\vec{0} = -\nabla p - en\left(\vec{E} + \frac{\vec{v} + \vec{u}}{c} \times \vec{B}\right) + \vec{R}, \tag{6}$$

$$\nabla \times \vec{B} = \frac{4\pi}{c}\vec{j}. \tag{7}$$

We use the Braginskii [36] expressions and notations for the ion–electron friction force $\vec{R}$ and electron heat flux $\vec{q}_e$. We assume small electron Hall parameter $\omega_e\tau_e = (eB/m_ec)\,\tau_e$, with $\tau_e \propto T^{3/2}/n$ being the electron collision time, hence,

$$\vec{R} = -\alpha_0 \frac{m_e n}{\tau_e}\vec{u} + \underbrace{\frac{\alpha_0''}{\delta_0}\frac{m_e n}{\tau_e}\left(\frac{e\tau_e\vec{B}}{m_ec}\right) \times \vec{u}}_{\text{Hall}} - \underbrace{\beta_0 n \nabla T}_{\text{Thermoelectric}} \underbrace{- \frac{\beta_0''}{\delta_0} n \left(\frac{e\tau_e\vec{B}}{m_e}\right) \times \nabla T}_{\text{Nernst}}, \tag{8}$$

$$\vec{q}_e = - \underbrace{\gamma_0 \frac{nT\tau_e}{m_e}\nabla T}_{\text{Spitzer heat flux}} \underbrace{- \frac{\gamma_0''}{\gamma_0\delta_0}\left(\frac{e\tau_e\vec{B}}{m_ec}\right) \times \left(\gamma_0 \frac{nT\tau_e}{m_e}\nabla T\right)}_{\text{Righi-Leduc}} + \underbrace{\beta_0 nT\vec{u}}_{\text{Thermoelectric}} \underbrace{+ \frac{\beta_0''}{\delta_0} nT \left(\frac{e\tau_e\vec{B}}{m_ec}\right) \times \vec{u}}_{\text{Ettingshausen}}. \tag{9}$$

We choose to rewrite $\gamma_0 nT\tau_e/m_e = \bar{K}T^{5/2}$, with $\bar{K}$ being the Spitzer conduction constant (we neglect the weak temperature and density dependence on the Coulomb logarithm) and m_e being the electron mass.

We now decompose every variable into base plus perturbation, and we assume small perturbations. The base variables are denoted with the subscript "0" and the perturbations with "1".

A. Base flow and normalization

We consider a one-dimensional steady base flow. The only component of the velocity is the streamwise component u_0, and we assume $\vec{B}_0 = \vec{0}$. We normalized every variable with the characteristic values n_c, T_c, and we choose as characteristic velocity the isothermal speed of sound, $u_c = \sqrt{T_c/\bar{m}}$. We define the characteristic length based on thermal conduction $L_c = 2\bar{K}T_c^{5/2}/5n_cu_c$. No

particular shape of the base variables is considered, but they are assumed to be sufficiently smooth and of the order of unity when normalized with these characteristic values.

B. Perturbed flow

We propose a modal decomposition in time and transversal coordinate for the perturbations, $\exp(i\omega t + ik_y y)$. We denote as v_1 the transverse velocity and b_1 the z component of the magnetic field normalized with a reference B_c obtained from the Biermann-battery term, $B_c = c\bar{m}u_c/eL_c$. In the linear stability analysis performed in this paper, the magnetic pressure, Hall and Ettingshausen terms are then dropped since they are proportional to $\left|\vec{B}\right|^2$. Besides, the thermoelectric effects cancel out when added up in Eq. (4), and the ion–electron friction becomes second order in this same equation.

The linearized and normalized governing equations become, in order,

$$i\omega n_1 + \frac{\mathrm{d}}{\mathrm{d}x}(n_0u_1 + n_1u_0) + ik_y n_0 v_1 = 0, \tag{10}$$

$$i\omega n_0u_1 + n_0u_0\frac{\mathrm{d}u_1}{\mathrm{d}x} + (n_1u_0 + n_0u_1)\frac{\mathrm{d}u_0}{\mathrm{d}x} = -\frac{\mathrm{d}p_1}{\mathrm{d}x}, \tag{11}$$

$$i\omega n_0v_1 + n_0u_0\frac{\mathrm{d}v_1}{\mathrm{d}x} = -ik_y p_1, \tag{12}$$

$$\begin{aligned} &i\omega\frac{3}{5}p_1 + \frac{\mathrm{d}}{\mathrm{d}x}(p_0u_1) + ik_y p_0v_1 + \frac{\mathrm{d}}{\mathrm{d}x}(u_0p_1) - \\ &\frac{2}{5}u_0\frac{\mathrm{d}p_1}{\mathrm{d}x} - \frac{2}{5}\frac{\mathrm{d}p_0}{\mathrm{d}x}u_1 = \left(\frac{\mathrm{d}^2}{\mathrm{d}x^2} - k_y^2\right)\left(T_0^{5/2}T_1\right) + \\ &ik_y b_1\left[c_R\frac{T_0^4}{n_0}\frac{\mathrm{d}T_0}{\mathrm{d}x} + \frac{c_H}{\mathrm{Re_m}}\left(p_0\frac{\mathrm{d}u_0}{\mathrm{d}x} + \frac{3}{5}u_0\frac{\mathrm{d}p_0}{\mathrm{d}x}\right)\right], \end{aligned} \tag{13}$$

$$\begin{aligned} &i\omega b_1 + \frac{\mathrm{d}}{\mathrm{d}x}(u_{\mathrm{net}}b_1) + i\frac{k_y}{n_0^2}\left(p_1\frac{\mathrm{d}n_0}{\mathrm{d}x} - n_1\frac{\mathrm{d}p_0}{\mathrm{d}x}\right) = \\ &\qquad\frac{1}{\mathrm{Re_m}}\left[\frac{\mathrm{d}}{\mathrm{d}x}\left(\frac{1}{T_0^{3/2}}\frac{\mathrm{d}b_1}{\mathrm{d}x}\right) - \frac{k_y^2}{T_0^{3/2}}b_1\right], \end{aligned} \tag{14}$$

with the density perturbation being related to pressure and temperature through the linearized equation of state

$$\frac{n_1}{n_0} = \frac{p_1}{p_0} - \frac{T_1}{T_0}. \tag{15}$$

In the left-hand side of the induction Eq. (14), we have the B-field convection due to the bulk plasma velocity and the Nernst term. We denote

$$u_N = -c_N\frac{T_0^{3/2}}{n_0}\frac{\mathrm{d}T_0}{\mathrm{d}x} \tag{16}$$

the normalized Nernst velocity, and

$$u_{\mathrm{net}} = u_0 + u_N \tag{17}$$

the net B-field convection velocity. In the right-hand side of the same equation, we have the magnetic-field diffusion. It is inversely proportional to the magnetic Reynolds number $\mathrm{Re_m} = u_cL_c/D_m$, with D_m being the characteristic magnetic diffusivity given by $D_m = \alpha_0c^2m_e/4\pi e^2n_c\tau_{ec} \propto T_c^{-3/2}$, and τ_{ec} is the characteristic electron collision time $\tau_{ec} \propto T_c^{3/2}/n_c$. Notice that the magnetic Reynolds number thereby defined is equivalent to the square of the ratio of the mean-free-path to collisionless skin depth Λ^2 used in the analysis by Bissell *et al.* [25].

It is important to highlight that, to the first order, the effect of the magnetic field on the hydrodynamics is restricted to the last two terms in square brackets in the energy Eq. (13), which act as a heat source. The first term corresponds to the Righi–Leduc, and the second one comes from the difference between electron and ion enthalpy convection, which is inversely proportional to $\mathrm{Re_m}$. The three numerical coefficients appearing in the the Righi–Leduc term (c_R), current enthalpy convection (c_H) and Nernst term (c_N) take the value $c_R = 5\gamma_0''/2\gamma_0^2\delta_0 \approx 1.71$, $c_H = 5/2\alpha_0\gamma_0 \approx 0.68$ and $c_N = 5\beta_0''/2\gamma_0\delta_0 \approx 1.83$ for $Z \gg 1$.

IV. LINEAR STABILITY ANALYSIS

The stability of the nonuniform system of Eqs. (10)–(14) is investigated in the small wavelength limit,

$$\epsilon \equiv \frac{1}{k_y} \ll 1, \tag{18}$$

by using the approach derived in Sec. A 4. As previously mentioned, a key point in the analysis is the correct estimation of the order of magnitude of the temporal frequency. To elucidate this, we first impose a modal decomposition of the variables in the streamwise coordinate as $\exp(-ik_x x)$, with $k_x \sim O(k_y)$ real. We obtain then the sheets $\omega_\alpha(k_x, k_y)$, $\alpha \in \{1, \ldots, 5\}$, identify which one leads to a convective instability, i.e., $\mathrm{Im}[\omega_\alpha(k_x, k_y)] < 0$, and take it as a reference for the estimation. This analysis, done in Sec. IV A, also serves to compare with previous criteria that classified the MTI as convective. With this estimation, we derive the conditions for the MTI to be absolute in Sec. IV B, which serves in turn to elucidate the stability of nonuniform coronal plasma profiles.

A. Frequency analysis: Criterion for convective instability

Let $\vec{q} = \{u_1, p_1, v_1, T_1, b_1\}^T$ denote the state variables vector. Considering a generic section $x = x^*$, imposing

the modal decomposition $\vec{q}(x) \sim \exp(-ik_x x)$, and introducing $\lambda \equiv k_x/k_y \sim O(1)$, the system of Eqs. (10)–(14) can be rewritten in a matrix form as

$$\omega B \cdot \vec{q} = \frac{1}{\epsilon^2} A(\epsilon, \lambda; x^*, \mathrm{Re_m}) \cdot \vec{q}. \tag{19}$$

Since the matrix B is diagonalizable, we introduce $C = B^{-1} \cdot A$. The condition for nontrivial solutions gives the equation for the frequencies ω,

$$\mathrm{Det}\left(C - \epsilon^2 \omega I_5\right) = 0, \tag{20}$$

where I_5 is the identity matrix in five dimensions.

We exploit the smallness of ϵ to solve Eq. (19). We make an initial estimation of the order of magnitude of the frequency as given by the energy equation, $\omega \sim \epsilon^{-2}$, and we rescale accordingly $\sigma = \epsilon^2 \omega$. The coronal plasma is highly conductive and the magnetic Reynolds number is typically large. We redefine then $\mathrm{re} = \epsilon^2 \mathrm{Re_m} \sim O(1)$, which will be justified *a posteriori*. We expand the matrix C, the eigenvalue σ and the eigenvector $\vec{q}$ as

$$C(\epsilon, \lambda; \mathrm{re}) = \sum_{j=0}^{j=\infty} \epsilon^j C_j(\lambda; \mathrm{re}), \quad \sigma = \sum_{j=0}^{j=\infty} \epsilon^j \sigma_j, \quad \vec{q} = \sum_{j=0}^{j=\infty} \epsilon^j \vec{q}_j, \tag{21}$$

respectively. Equation (19) becomes

$$\sum_{j=0}^{j=\infty} \epsilon^j \left[\sum_{k=0}^{k=j} (C_k - \sigma_k I_5) \cdot \vec{q}_{j-k} \right] = 0. \tag{22}$$

Solving independently for every order of ϵ yields a hierarchy of equations to systematically derive the eigenvalues σ_i and eigenvectors $\vec{q}_i$.

The leading order of the frequencies, σ_0, corresponds to the eigenvalues of the matrix C_0, which yields two different values, $\sigma_{0_1} = i5\left(1+\lambda^2\right) T_0^{5/2}/3n_0$ and $\sigma_{0_2} = 0$. The first one is directly related to the energy equation (thermal conduction pole) and corresponds to a stable root (positive imaginary part). The latter eigenvalue has algebraic and multiplicity equal to four, and spans a four-dimensional vector space $\{Z_j, j = 1, 4\}$ where the temperature is unperturbed. We must explore higher-order terms to determine the character of it.

The order ϵ of Eq. (22) gives

$$(C_1 - \sigma_1 I_5) \cdot \vec{q}_0 + (C_0 - \sigma_0 I_5) \cdot \vec{q}_1 = 0. \tag{23}$$

For a given σ_0 , left multiplying by the corresponding $\vec{q}_0^T$ yields an equation for σ_1. This works straightforwardly if the multiplicity of the eigenvalue is one. For eigenvalues with larger multiplicity, the method differs slightly as multiplying by any combination of the corresponding eigenvectors would give a different value of σ_1. Instead, the condition to be imposed is $\mathrm{Det}\,(M) = 0$, where M is the matrix with entries

$$M_{ij} = Z_i^T \cdot (C_1 - \sigma_1 I_5) \cdot Z_j, \tag{24}$$

and Z_i are a basis of the vector space spanned by the eigenvalue $\sigma_{0_2} = 0$. Applying this procedure to our problem splits this eigenvalue into four different ones at the next order σ_1. They correspond to vorticity, acoustic (two) and induction poles. They are purely oscillatory and are shown, together with the thermal pole, in Table I. The eigenvector $\vec{q}_0$ related to each eigenvalue is shown in Table II.

Pole	First nonzero eigenvalue	Features
Vorticity	$\sigma_1 = \lambda u_0$	Incompressible
Acoustic (I)	$\sigma_1 = \lambda u_0 - \sqrt{T_0(\lambda^2+1)}$	Potential
Acoustic (II)	$\sigma_1 = \lambda u_0 + \sqrt{T_0(\lambda^2+1)}$	Potential
Thermal	$\sigma_0 = i\dfrac{5\left(\lambda^2+1\right)T_0^{5/2}}{3n_0}$	$T_1 \neq 0$
Induction	$\sigma_1 = \lambda u_{\mathrm{net}}$	B-field dominated

Table I. First nonzero eigenvalue of the frequencies.

Pole	u_1	p_1	v_1	T_1	b_1
Vorticity	1	0	λ	0	0
Acoustic (I)	$-\lambda$	$n_0\sqrt{T_0(\lambda^2+1)}$	1	0	$\dfrac{-\mathrm{d}\log T_0/\mathrm{d}x}{1+\lambda\frac{u_N}{\sqrt{T_0(\lambda^2+1)}}}$
Acoustic (II)	$-\lambda$	$-n_0\sqrt{T_0(\lambda^2+1)}$	1	0	$\dfrac{-\mathrm{d}\log T_0/\mathrm{d}x}{1-\lambda\frac{u_N}{\sqrt{T_0(\lambda^2+1)}}}$
Thermal	0	n_0	0	1	0
Induction	0	0	0	0	1

Table II. Leading order of the eigenvector $\vec{q}_0$ for each pole.

The induction pole, to the leading order, stands for net B-field convection as given by the Nernst and plasma blowoff velocities, $\sigma_1 = \lambda u_{\mathrm{net}}$. It is necessary to derive higher-order terms to elucidate its stability. The order ϵ^2 of Eq. (22) gives

$$(C_2 - \sigma_2 I_5) \cdot \vec{q}_0 + (C_1 - \sigma_1 I_5) \cdot \vec{q}_1 + (C_0 - \sigma_0 I_5) \cdot \vec{q}_2 = 0. \tag{25}$$

Left multiplying by the induction eigenvector (see Table II) allows one to obtain the term σ_2, which is purely imaginary:

$$i\sigma_2 = -\frac{\mathrm{d}u_{\mathrm{net}}}{\mathrm{d}x} - \frac{\lambda^2+1}{\mathrm{re}T_0^{3/2}} + c_R\frac{T_0^{5/2}}{n_0}\frac{\mathrm{d}\log T_0}{\mathrm{d}x}\cdot \left(\frac{1}{\lambda^2+1}\frac{\mathrm{d}\log n_0}{\mathrm{d}x} + \frac{1}{\lambda^2+1-\lambda^2\dfrac{u_N^2}{T_0}}\frac{\mathrm{d}\log T_0}{\mathrm{d}x}\right). \quad (26)$$

The criterion for convective instability would require the imaginary part of the induction mode to be negative. Rearranging terms, the following criterion is obtained

$$-\omega_i = \frac{T_0^{5/2}}{n_0}\left\{\left[\frac{k_y^2}{k_x^2+k_y^2-k_x^2\left(c_N\dfrac{T_0}{n_0}\dfrac{\mathrm{d}T_0}{\mathrm{d}x}\right)^2}c_R + \frac{5}{2}c_N\right]\left(\frac{\mathrm{d}\log T_0}{\mathrm{d}x}\right)^2 + c_N\frac{\mathrm{d}^2\log T_0}{\mathrm{d}x^2} + \left(\frac{k_y^2}{k_x^2+k_y^2}c_R - c_N\right)\frac{\mathrm{d}\log T_0}{\mathrm{d}x}\frac{\mathrm{d}\log n_0}{\mathrm{d}x}\right\} - \frac{\mathrm{d}u_0}{\mathrm{d}x} - \frac{k_x^2+k_y^2}{\mathrm{Re_m}T_0^{3/2}} > 0. \quad (27)$$

The induction pole is in essence the one responsible for the MTI. Inequality (27) states that a localized perturbation arising in a region of the corona where this is satisfied will grow with a time scale of order unity while drifting with the group velocity equal to u_{net}.

Although Eq. (27) is more practical for straightforward application, more physical insight is obtained from analysis of Eq. (26). The first term in the right-hand side stands for B-field stretching. A negative net convection derivative would accumulate magnetic field favoring the development of the instability. The second term corresponds to B-field diffusion, which inhibits the instability growth. We see that the scaling $\mathrm{Re_m} \sim O\left(k_y^2\right)$ is required for diffusivity not to damp the instability completely. The third term stands for the cross product between the Righi–Leduc and the Biermann battery terms, the driving mechanisms of this instability. Although gradients of temperature and density in the same direction contribute to the MTI, it is not a necessary condition.

For comparison and application purposes, it is useful to rewrite the frequency related to the induction mode in dimensional quantities as:

$$\omega = k_x u_{\mathrm{net}} - i\frac{\tau_e T_0}{m_e}\left\{\left[\frac{k_y^2}{k_x^2+k_y^2-k_x^2\left(\dfrac{u_{\mathrm{N}}}{c_s}\right)^2}\frac{\gamma_0''}{\gamma_0\delta_0} + \frac{5}{2}\frac{\beta_0''}{\delta_0}\right]\left(\frac{\mathrm{d}\log T_0}{\mathrm{d}x}\right)^2 + \frac{\beta_0''}{\delta_0}\frac{\mathrm{d}^2\log T_0}{\mathrm{d}x^2} + \left(\frac{k_y^2}{k_x^2+k_y^2}\frac{\gamma_0''}{\gamma_0\delta_0} - \frac{\beta_0''}{\delta_0}\right)\frac{\mathrm{d}\log T_0}{\mathrm{d}x}\frac{\mathrm{d}\log n_0}{\mathrm{d}x}\right\} + i\frac{\mathrm{d}u_0}{\mathrm{d}x} + iD_m T_c^{3/2}\frac{k_x^2+k_y^2}{T_0^{3/2}}. \quad (28)$$

In this expression, the Nernst velocity takes the dimensional form $u_N = (\beta_0''\tau_e/\delta_0 m_e)\,\mathrm{d}T_0/\mathrm{d}x$, and $c_s = \sqrt{T_0/\bar{m}}$ refers to the local (isothermal) speed of sound.

Comparison with previous criteria

The condition for convective instability, Eq. (27), is a more complete criterion compared to those derived in previous analyses, Refs. [15, 16, 20–22]. In the seminal paper by Tidman and Shanny [15], the condition for instability only required gradients of temperature and density to be parallel, $(\mathrm{d}T_0/\mathrm{d}x)\,(\mathrm{d}n_0/\mathrm{d}x) > 0$. However, neither the Nernst term nor the plasma hydrodynamics were considered in their derivation.

In the analysis by Dolginov and Urpin [20], the Nernst term was taken into account, but the authors did not include the ablative plasma motion (blowoff velocity). Their results, Eqs. (16) and (19) in their paper, can be retrieved from Eq. (28) by setting $u_0 = 0$ and taking $Z = 1$ for the Braginskii's transport coefficients. Their analysis was based on the asymptotic limits (large and small) of the phase velocity normalized with the speed of sound $\zeta = \omega^2/\left(k_x^2+k_y^2\right)c_s^2$. In the perturbation method employed in this work, we have shown that, to the leading order, the induction mode is $\omega = k_x u_{\mathrm{net}}$. Consequently, we find $\zeta \sim \left(u_N/c_s\right)^2$ if we take a null blowoff velocity. Interestingly, in the context of a coronal plasma, the characteristic length is based on thermal conduction at the critical surface, which makes $u_{\mathrm{N}} \sim c_s$ and hence $\zeta \sim O\,(1)$.

The effect of a base flow velocity was taken into account in the analyses performed by Ogasawara *et al.* [21] and Hirao and Ogasawara [22]. The authors restricted the analysis to $k_x = 0$ perturbations ($k_z = 0$ in their nomenclature). In the first paper, Ref. [21], the Nernst term was omitted. The marginal stability condition, Eq. (4.1) in the reference, can be retrieved from Eq. (28) by setting $k_x = 0$ and $\beta_0'' = 0$. The authors emphasized the stabilizing role of the expanding plasma, $\mathrm{d}u_0/\mathrm{d}x > 0$, in addition to magnetic diffusion, in the supersonic, low-density region of the corona. The effect of the Nernst

term was included in the second paper, Ref. [22], although the flow velocity was set to 0 in the final step of derivation of the growth rate. Similarly to Dolginov and Urpin, the authors defined two regimes depending on the the asymptotic value of the normalized phase velocity, yielding similar conditions for the marginal stability condition.

B. Mode analysis: Criterion for absolute instability

We have identified the induction pole as the one responsible for the MTI. The real part of the temporal frequency is $\omega_r = k_x u_{\rm net}$ and the imaginary part is given by Eq. (27). The net B-field convection velocity $u_{\rm net}$ becomes therefore the governing parameter as it dictates the order of magnitude of the temporal frequency. We can distinguish between two cases: perturbations developing in regions where the net velocity is finite, $u_{\rm net} \sim O(1)$, and perturbations developing in regions where the net velocity is small, $|u_{\rm net}| \lesssim k_y^{-1}$. In the former case the real part of the frequency of the induction mode is predominant and we have $\omega \sim O(k_y)$, while in the latter it is the imaginary part the predominant and we have $\omega \sim O(1)$.

We consider first a finite net convection velocity. Ordering accordingly $\tilde{\omega} = \omega/k_y\sqrt{T_0} \sim O(1)$, introducing the isothermal Mach number ${\rm Ma} = u_0/\sqrt{T_0}$, the dispersion relation Eq. (A.19) related to the system of Eqs. (10)–(14) yields

$$(\lambda {\rm Ma} - \tilde{\omega})\left(\lambda\frac{u_{\rm net}}{\sqrt{T_0}} - \tilde{\omega}\right)\left(\lambda^2+1\right)\cdot \left[\lambda^2 + 1 - (\lambda {\rm Ma} - \tilde{\omega})^2\right] = 0. \quad (29)$$

This expression describes the modes of the linearized magnetohydrodynamic equations without any coupling term (energy source); in order: vortical, induction, thermal and acoustic poles. It does not satisfy the absolute instability criterion as every pole merger $\lambda(\bar{\omega})$ taking place for negative Im $(\bar{\omega})$ corresponds to poles coming from the same half in the Fourier space.

The situation is different in regions where the net convection velocity is small, $|u_{\rm net}| \lesssim k_y^{-1}$. In this case, the roots translate in the Fourier space for frequency changes of order unity. Rescaling accordingly

$$\bar{\omega} = \frac{\omega}{c_R\dfrac{T_0^{5/2}}{n_0}\left(\dfrac{{\rm d}\log T_0}{{\rm d}x}\right)^2}, \quad \bar{\rm re} = {\rm Re_m}\frac{c_R}{k_y^2}\frac{T_0^4}{n_0}\left(\frac{{\rm d}\log T_0}{{\rm d}x}\right)^2, \quad (30)$$

the dispersion relation Eq. (A.19) related to the system of Eqs. (10)–(14) yields:

$$\left(i\bar{\omega} + \frac{\lambda^2+1}{\bar{\rm re}}\right)\left(\lambda^2+1\right)\left[\lambda^2\left(1-{\rm Ma}^2\right)+1\right] = \left(\lambda^2+1\right) + (\delta-1)\left[\lambda^2\left(1-{\rm Ma}^2\right)+1\right], \quad (31)$$

where we have introduced the parameter characterizing the orientation between pressure and temperature gradients

$$\delta = \frac{{\rm d}\log p_0}{{\rm d}\log T_0}. \quad (32)$$

For simplicity, we have assumed a stronger ordering $|u_{\rm net}| \ll k_y^{-1}$ when deriving Eq. (31). Its right-hand side represents the coupling between the Biermann-battery and the Righi–Leduc terms and acts as a forcing term.

The dispersion relation depends on λ^2, hence the poles can be grouped into three pairs. For Im $(\bar{\omega}) \to -\infty$, we identify the thermal poles, $\lambda^2 = -1$, the acoustic poles, $\lambda^2 = 1/\left({\rm Ma}^2 - 1\right)$, and the diffusive poles, $\lambda^2 = -i\bar{\omega}\bar{\rm re} \to -\infty$. It also follows that $\lambda = 0$ stands for a merger point regardless of the value of $\bar{\rm re}$, δ, and Ma. As a side note, we remark that there is a seventh root related to the vortical motion of the flow which is placed at $\lambda = 0$ for any $i\bar{\omega}$, and therefore not considered in the analysis. The merger takes place for a frequency $\bar{\omega}_{M_0} \equiv \bar{\omega}|_{\lambda=0}$ that reads

$$i\bar{\omega}_{M_0} = \delta - \frac{1}{\bar{\rm re}}. \quad (33)$$

This merger qualifies for absolute instability if $i\bar{\omega}_{M_0} > 0$ or, equivalently, if pressure and temperature gradients are parallel, $\delta > 0$. Since the merger takes place at the origin, $\lambda = 0$, the perturbation would develop an anisotropic structure with a larger streamwise length scale because $k_x \ll k_y$. However, this merger is not likely to take place in coronal plasmas. The requirement of small $u_{\rm net}$ forces temperature to be an increasing function with radial distance so that the Nernst velocity cancels the blowoff velocity. Since pressure in the corona is typically a decaying function of radial distance, see for example Fig. 5 in Sec. V, we have that $\delta < 0$ wherever $u_{\rm net}$ is small.

The merger at the origin is not the only one that occurs. Additional mergers take place in the parametric region defined as $\delta/(\delta-1) < {\rm Ma}^2 < 1 \cup \delta < {\rm Ma}^2 < 1$. In this case, the poles $\lambda(\bar{\omega})$ translate in the Fourier space as sketched in Fig. 2. We discuss the case $\bar{\rm re} \to \infty$ for convenience. Each thermal pole merges with an acoustic pole at $\lambda = \pm\lambda_{M_1}$, on the imaginary axis, split then into poles with opposite real part that travel toward the real axis, where they merge again with their complex conjugate at $\lambda = \pm\lambda_{M_2}$. From this point on, one pole per pair of complex conjugates moves inward and merges again at the origin for the aforementioned frequency $\bar{\omega}_{M_0}$. It can be seen that the merger M_2 also satisfies the criterion for absolute instability and creates another branch in the Laplace space. This takes place at a temporal growth

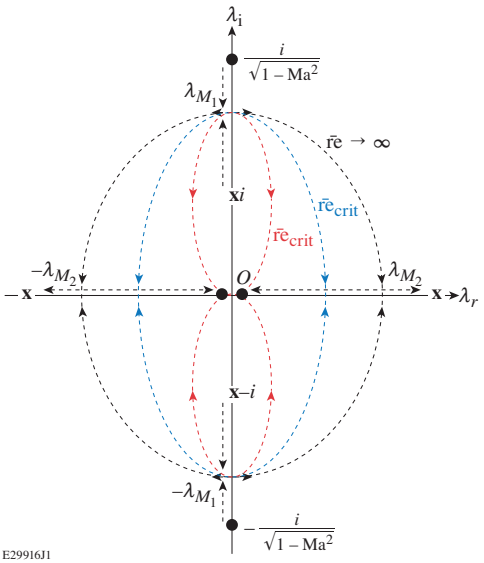

Figure 2. Translation of the acoustic (circles) and thermal (triangles) poles of the dispersion relation Eq. (31) in the Fourier space. The arrows in black represent the mapping of the poles when the frequency varies from $i\bar{\omega} \to \infty$ to $i\bar{\omega} = \delta$, and $\bar{r}e \to \infty$. The mapping sketched by the arrows in blue and red correspond to $\bar{r}e = \bar{r}e_{\mathrm{crit.}}$ and $i\bar{\omega}$ varying from ∞ to 0. Blue case assumes $\mathrm{Ma}^2 > 2\delta$, while the red corresponds to $\mathrm{Ma}^2 = 2\delta$.

rate we denote as $i\bar{\omega}_{M_2}$, which is higher than and therefore predominant to $i\bar{\omega}_{M_0}$. Its value is obtained from differentiating Eq. (31) with respect to λ^2, yielding

$$i\bar{\omega}_{M_2} = \delta - 1 + \frac{2 - \delta - 2\sqrt{(1-\delta)\left(1-\mathrm{Ma}^2\right)}}{\mathrm{Ma}^2}, \quad (34)$$

and is computed in Fig. 3. This expression is smaller than unity, but larger than $i\bar{\omega}_{M_0}$, in the parametric region considered. The structure developed by the perturbation would be given by the wavelength aspect ratio $|\lambda_{M_2}|$. It ranges from filamentary structures with predominant longitudinal scale length in the region $\mathrm{Ma}^2 \approx \delta$, where we have $|\lambda_{M_2}| = \left[\left(\mathrm{Ma}^2 - \delta\right)/2\delta\left(1-\delta\right)\right]^{1/2} \ll 1$, to structures with predominant transversal scale length close to the sonic boundary $\mathrm{Ma}^2 \approx 1$, where we have $|\lambda_{M_2}| = \left[\left(1-\delta\right)/\left(1-\mathrm{Ma}^2\right)\right]^{1/4} \gg 1$.

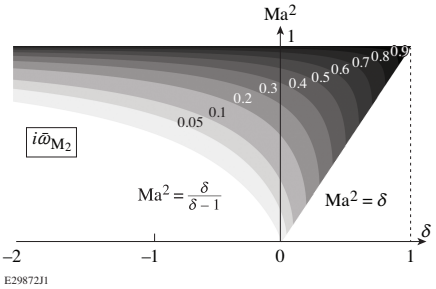

Figure 3. Isocontours of the temporal growth rate $i\bar{\omega}_{M_2}$ in the phase space isothermal Mach number Ma and pressure-to-temperature gradient ratio $\delta = \mathrm{d}\log p_0/\mathrm{d}\log T_0$.

The merger M_2 is of relevance for coronal plasmas as it shows that the MTI can be absolute in conditions where pressure and temperature gradients are antiparallel ($\delta < 0$). When rewritten in dimensional form, the growth rate γ_{MTI} is given by

$$\gamma_{\mathrm{MTI}_{\mathrm{ns}^{-1}}} = 0.19 i\bar{\omega}_{M_2} \frac{10}{\log\Lambda} \frac{\gamma_0''}{\gamma_0 \delta_0 Z} \frac{T_{\mathrm{keV}}^{5/2}}{n_{10^{22}\mathrm{cm}^{-3}}} \left(\frac{\mathrm{d}\log T}{\mathrm{d}x_{100\mu\mathrm{m}}}\right)^2, \quad (35)$$

where $\log\Lambda$ stands for the Coulomb logarithm and $i\bar{\omega}_{M_2}\left(\mathrm{Ma}^2, \delta\right)$ is given by Eq. (34). This exponential growth rate indicates the asymptotic temporal behavior, in the limit of short perturbation wavelength $k_y \gg 1$ and in the absence of diffusive terms, of a localized perturbation developing in a region satisfying the absolute MTI criterion. Such perturbation will grow *in situ* in the frame of reference of the imploding shell and can affect the implosion dynamics. Notice that, in contrast to previous growth rates derived in a convective instability analysis [Eqs. (15) and (18) in Dolginov and Urpin [20], Eqs. (3) in Bissell *et al.* [24] and Eqs. (17) and (18) in Bissell *et al.* [25]], expression (35) does not depend on an arbitrary choice of the perturbation streamwise wavenumber k_x. Instead, imposing the absolute instability condition provides the spatial structure that such localized perturbation develops, given by the merging point

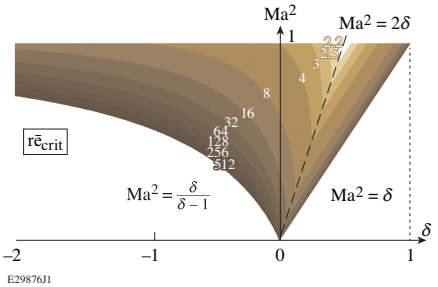

Figure 4. Isocontours of the critical magnetic Reynolds number in the phase space isothermal Mach number Ma and pressure-to-temperature gradient ratio $\delta = \mathrm{d}\log p_0/\mathrm{d}\log T_0$.

in the Fourier space $|\lambda_{M_2}| = k_x/k_y$.

The growth rate Eq. (35) has been derived in the absence of magnetic diffusion. Considering a finite $\bar{\mathrm{re}}$ modifies the trajectory of the poles by bringing λ_{M_2} closer to the origin and thus reducing $i\bar{\omega}_{M_2}$. We can identify a critical Reynolds number $\bar{\mathrm{re}}_{\mathrm{crit}}$ for which the merger M_2 occurs for $i\bar{\omega}_{M_2} = 0$, computed in Fig. 4. In the particular case $\mathrm{Ma}^2 = 2\delta$, the merger takes place at the origin for $\bar{\mathrm{re}} = \bar{\mathrm{re}}_{\mathrm{crit}}$ (see Fig. 2). Hence, in the region $\delta < \mathrm{Ma}^2 < 2\delta \cap \mathrm{Ma}^2 \leq 1$, we define $\bar{\mathrm{re}}_{\mathrm{crit}}$ such that for $\bar{\mathrm{re}} < \bar{\mathrm{re}}_{\mathrm{crit}}$, λ_{M_2} becomes imaginary and this branch ceases to exist. We can derive the cutoff wavenumber based on $\bar{\mathrm{re}}_{\mathrm{crit}}$ as

$$\frac{k_{y_c}}{\dfrac{\mathrm{d}\log T}{\mathrm{d}x}} = 27.5\frac{10}{\log\Lambda}\sqrt{\frac{\gamma_0''}{\gamma_0\delta_0\alpha_0 Z^2}}\frac{T_{\mathrm{keV}}^2}{\left(n_{10^{22}\mathrm{cm}^{-3}}\bar{\mathrm{re}}_{\mathrm{crit.}}\right)^{1/2}}. \quad (36)$$

Following the arguments exposed in Sec. A 4, we can extend the analysis to nonuniform plasma profiles. If the net convection velocity u_{net} is small in a wide region of the profile, the WKB method yields a problem with two turning points. Accordingly, the growth rate will be given by the "most unstable section," that is, the section where Eq. (35) evaluates to its maximum. Given the strong dependence of $i\bar{\omega}_{M_2}$ on the Mach number, the most unstable section typically corresponds to the isothermal sonic point, $\mathrm{Ma} = 1$, where $i\bar{\omega}_{M_2} \approx 1$. Furthermore, in this section the requirement over the pressure and temperature scale lengths is relaxed as any $\delta > -\left(1 - \mathrm{Ma}^2\right)^{-1}$ falls within the parametric region considered. The large values of the perturbation aspect ratio $|\lambda_{M_2}|$ near the sonic point suggest the formation of elongated structures in the transversal direction. Of interest is the critical magnetic Reynolds number in the sonic point, which can be obtained analytically $\bar{\mathrm{re}}_{\mathrm{crit}} = 4\,(1-\delta)$. When considering magnetic diffusivity, the perturbation aspect ratio can be reduced to $|\lambda_{M_2}| = \sqrt{1-2\delta}$ when $\bar{\mathrm{re}} = \bar{\mathrm{re}}_{\mathrm{crit}}$.

We can then infer the criterion for MTI in coronal plasmas: if u_{net} is small in a neighborhood around the isothermal sonic point, the coronal plasma is MTI unstable to short-wavelength perturbations larger than the cutoff given by Eq. (36).

V. APPLICATION TO DIRECT-DRIVE IMPLOSIONS

We assess the occurrence of the MTI in direct-drive implosions using 1-D simulations from the radiation hydrocode *LILAC* [37]. Figure 5 shows velocity profiles of a 3.28-mm-diameter target implosion driven by a 2-MJ energy, 350-TW peak power laser pulse. Initially, the 307-μm-thick deuterium–tritium (DT) ice shell is encased by a 32-μm-thick plastic (CH) ablator. At the particular time step plotted, the DT–CH interface is placed within the conduction layer. Due to the strong dependence of the Nernst velocity on the atomic number, two structures can be observed in it. In the region filled with CH, the Nernst velocity overcomes the blowoff velocity. This region is being pushed away by the ablated DT, where the weaker Nernst velocity can barely cancel the blowoff velocity. This results in the formation of a wide region of low B-field convection velocity, which includes the sonic point, making the conditions for absolute instability applicable.

The conditions for absolute magnetothermal instability are satisfied during a significant lapse of time. In Fig. 6, the net convection velocity is shown for different time steps. At $t = 15.7$ ns, the ablation front just penetrates into the DT, hence all the conduction layer is CH. The Nernst velocity dominates and we have $|u_{\mathrm{net}}/u_0| \sim 0.5$ at the isothermal sonic point. For later times, the DT ablates and sweeps away the CH material from the conduction zone. During this process, $|u_{\mathrm{net}}/u_0|$ remains small in the neighborhood around the isothermal sonic point.

Figure 7 shows the growth rate γ_{MTI} computed at times satisfying $|u_{\mathrm{net}}/u_0| < 1/2$ at the isothermal sonic point using Eq. (35) in this section. This condition is verified in the last two thirds of the peak laser power time frame, beginning at the moment when the ablation front penetrates into the DT. The growth rate decreases from $\gamma_{\mathrm{MTI}} = 1.4\ \mathrm{ns}^{-1}$ to $\gamma_{\mathrm{MTI}} = 0.3\ \mathrm{ns}^{-1}$ by the end

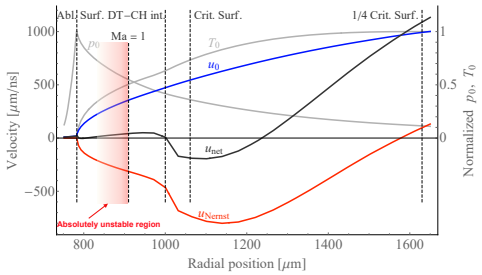

Figure 5. Profiles of the plasma blowoff velocity u_0, Nernst velocity u_N and net convection velocity $u_{\rm net}$ in the conduction layer of a standard 2MJ direct drive LILAC simulation. The laser profile corresponds to Fig. 7 (top) and the snapshot shown is $t = 16.5$ ns. The electron temperature T_0 and total pressure p_0 profiles have been normalized with their maximum value, 4.4 keV and 161 Mbar, respectively. The most unstable section of the profile corresponds to the isothermal sonic point Ma = 1.

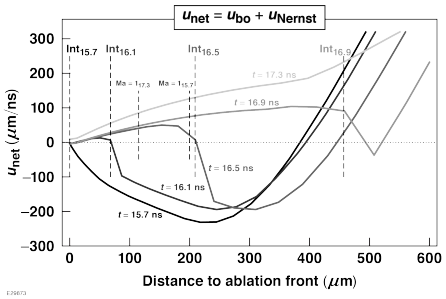

Figure 6. Profiles of the net convection velocity $u_{\rm net}$ at different time steps obtained from the 2MJ laser energy simulation. The spatial reference is set at the respective ablation front position. The profile for $t = 16.5$ ns is the same as plotted in Fig. 5. The dashed lines show the interface between DT and CH materials. The dot-dashed lines show the isothermal Mach point.

of the pulse, resulting in perturbations undergoing 2.34 e-foldings ($\sim 10\times$ amplification).

Since the growth rate is given by the flow conditions at the sonic region, it scales as the speed of sound divided by the conduction length, being both strong functions of the laser intensity [13, 38]. Consequently, $\gamma_{\rm MTI}$ should be invariant for hydro-equivalent implosions [39]. In the same Fig. 7, calculations for a 30-kJ hydro-equivalent implosion show growth rates varying from $\gamma_{\rm MTI} = 3.2$ ns^{-1} to $\gamma_{\rm MTI} = 1.2$ ns^{-1} in a time interval of 0.5 ns, resulting in 1.36 e-foldings ($\sim 4\times$ amplification). Larger-size hydro-equivalent implosions are therefore more susceptible to the MTI since the implosion time scales with the target

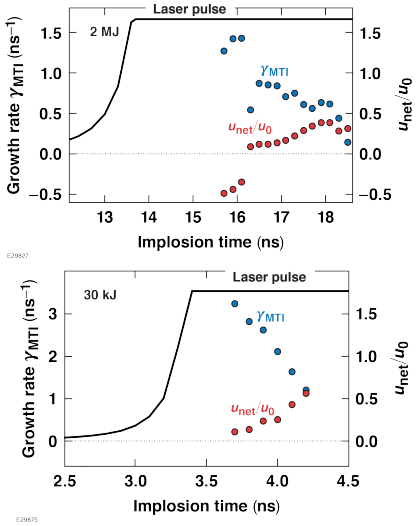

Figure 7. Maximum growth rate $\gamma_{\rm MTI}$ computed from Eq. (35) and velocity ratio $u_{\rm net}/u_0$ at the isothermal sonic point for a 2 MJ (top) and 30 kJ (bottom) direct-drive implosions. Laser power pulse shape is plotted for reference. End of laser pulses: 18.5 ns and 4.5 ns, respectively.

diameter. Both simulations showed cutoff wavelength of 10μm (2MJ case) and 14μm (30kJ case) during the time interval that the MTI is active.

A brief remark about the validity of the model employed. Sherlock and Bissell [34] recently reported that non locality significantly suppresses the Biermann battery, and provided a useful correction when these effects are important. We found that this correction is not necessary for the growth rates derived in this work, as they are given by the plasma conditions at the sonic point within the conduction layer, which is collisional. For example, in the 2MJ simulation, the electron temperature and density at this section are 2.2 keV and 1.65×10^{22}cm^{-3}, respectively, which yields an electron mean free path $\sim 8\mu$m, smaller than the temperature scale length $\sim 320\mu$m. On another matter, we have used Braginskii's expressions and coefficients for the transport terms. Recently, Davies *et al.* [40] and Sadler *et al.* [41] provided new fits that corrected Braginskii's fits and solved subtle inaccuracies of the improved fits by Epperlein and Haines [42] and Ji and Held [43]. The correction of interest with application to this work is the underestimation that Braginskii made of the Nernst velocity coefficient. Although it is a small difference (up to a 10% at small Hall parameters) and does not undermine the soundness of this analysis, it should be taken into account in future numerical analysis. As mentioned in Davies *et al.* [40]: "the physics of interest often depends

on small differences between the Nernst and flow velocities, so this underestimate can be significant," which is the case for the MTI.

VI. CONCLUSION AND DISCUSSION

In this paper, we have derived the conditions under which the magnetothermal instability (MTI) is absolute and its implication on the stability of nonuniform coronal plasmas in the short-perturbation wavelength ($k_y \gg 1$) regime.

First, we have reviewed the criteria for convective and absolute instability in uniform systems and applied this theory to a slab of coronal plasma. The coronal plasma is convectively unstable, i.e., it supports unstable waves if the condition in Eq. (27) is satisfied. This condition shows that the coronal plasma can amplify perturbations given by external sources while they drift away from it following the net B-field convection velocity $u_{\rm net}$ (sum of the plasma flow and Nernst velocities). Second, the more restrictive absolute instability criterion has been applied. Absolute instabilities correspond to spatial resonances inherent to the coronal plasma and as such does not require of an external source. We have found that the MTI can be absolute if $u_{\rm net}$ is small and the temperature and pressure scale length ratio falls within the parametric region defined in Fig. 3. The MTI growth rate is then given by Eq. (35) in the absence of magnetic diffusion. The inclusion of magnetic diffusion can stabilize the MTI for perturbation wavenumbers higher than the cutoff derived in Eq. (36).

We have reviewed, in Sec. A 4, that the occurrence of absolute instability is intrinsically related to the stability of nonuniform profiles to short-wavelength perturbations, in our case coronal plasmas. The growth rate is given by the most unstable section of the flow, which typically corresponds to the isothermal sonic point. The condition for MTI is then reduced to $u_{\rm net}$ being small at the sonic point. We have shown that this requirement can be satisfied in direct-drive implosions during a significant part of the laser pulse duration. Application to ICF direct-drive implosions suggests that the growth rate of the MTI is a strong function of the laser intensity and remains approximately the same for hydro-equivalent implosions (of the order of a few gigahertz in a generic OMEGA laser design). Consequently, the MTI is more detrimental when considering larger-size, hydro-equivalent implosions.

This theory reveals a picture of the MTI where the conduction layer is the dynamically active region of the corona. Here is found the spatial resonance that causes perturbations to grow *in situ,* hence traveling with the imploding shell and potentially altering its dynamics. We have seen that the structure of the unstable perturbations tends to elongated filaments in the azimuthal direction. They can spread out to regions of outflowing $u_{\rm net}$, being subsequently stretched radially and filling the outer corona. Such a picture is in qualitative agreement with some of the analyses inferred in the literature from the radiographic images of direct-drive implosions. Particularly, ripple structures with predominant azimuthal scale length were shown by Igumenshchev *et al.* [44]. More importantly, Rygg *et al.* [5] reported that the striated fields originate close to the capsule surface, and conjectured that the vast spatial extent of these fields reflects an outward convection of filamentary structures originally produced inside the critical surface.

Finally, the application of this theory to ICF implosions provide an MTI growth rate in the range of a fraction to few gigahertz, which is milder than the ones discussed by Manuel *et al.* [7] and Bissell *et al.*[25] (several to tens of gigahertz). This is mainly due to authors employing growth rate expressions derived from a convective instability analysis, which favors lower-density, higher-temperature regions (outer corona) as more unstable regions. The outer corona indeed supports unstable waves, but we deem we must impose the requirement for absolute instability to account how the MTI affects the dynamics of the implosion. This holds the plasma state at the conduction layer responsible of the growth rate of the MTI.

ACKNOWLEDGEMENTS

F. García-Rubio thanks Dr. Davies, Dr. Cao and Dr. Goncharov for insightful discussions pertaining to the simulations. This work is supported by the Department of Energy Office of Science, Fusion Energy Sciences program grants DE-SC0016258, DE-SC0014318 and DE-SC0021072. F. García-Rubio was also supported by the Advanced Research Projects Agency-Energy (ARPA-E), U.S. Department of Energy, under Award No. DE-AR0001272. J. Sanz was also supported by the Spanish Ministerio de Economía y Competitividad, Project No. RTI2018-098801-B-I00. H. Aluie was also supported by US DOE grants DE-SC0020229, DE-SC0019329, US NASA grant 80NSSC18K0772, US NSF grants OCE-2123496, PHY-2020249 and US NNSA grants DE-NA0003856, DE-NA0003914. This material is based upon work supported by the Department of Energy National Nuclear Security Administration under Award Number DE-NA0003856, the University of Rochester, and the New York State Energy Research and Development Authority. This report was prepared as an account of work sponsored by an agency of the U.S. Government. Neither the U.S. Government nor any agency thereof, nor any of their employees, makes any warranty, express or implied, or assumes any legal liability or responsibility for the accuracy, completeness, or usefulness of any information, apparatus, product, or process disclosed, or represents that its use would not infringe privately owned rights. Reference herein to any specific commercial product, process, or service by trade name, trademark, manufacturer, or otherwise does not necessarily constitute or imply its endorsement, recommendation, or favoring by

the U.S. Government or any agency thereof. The views and opinions of authors expressed herein do not necessarily state or reflect those of the U.S. Government or any agency thereof.

Appendix A: Review of the stability of uniform systems

In this Appendix, we recap the stability of uniform, time-invariant linear systems, following closely the analysis made in Briggs [30]. Let $u(t,x)$ represent the state of such system, often referred to as perturbation, we focus on the asymptotic behavior in time of

$$\mathcal{L}\left(\frac{\partial}{\partial t},\frac{\partial}{\partial x}\right)\circ u(t,x)=s(t,x),\qquad u(0,x)=0. \tag{A.1}$$

Here, $\mathcal{L}$ represents the linear differential operator with constant coefficients that characterizes the system, and $s(t,x)$ is the source of excitation. The causality condition demands that $s(t,x)=0$ for $t<0$. Note that any initial condition $u_0(x)$ could be reabsorbed in the source term $s(t,x)$ by redefining $v(t,x)=u(t,x)-u_0(x)$.

Fourier and Laplace analysis tools are well suited to characterize the stability of these systems. In order to keep the same nomenclature as in Ref. [30], we define the Fourier and Laplace transformations as

$$g(k)=\int_{-\infty}^{+\infty}g(x)\exp(ikx)\,\mathrm{d}x, \tag{A.2}$$

$$f(\omega)=\int_{0}^{+\infty}f(t)\exp(-i\omega t)\,\mathrm{d}t, \tag{A.3}$$

respectively.

1. Green's function formalism

The Green's function $G(t-\tau,x-\eta)$ corresponding to a system governed by Eq. (A.1) satisfies

$$\mathcal{L}\left(\frac{\partial}{\partial t},\frac{\partial}{\partial x}\right)\circ G(t-\tau,x-\eta)=\delta(t-\tau,x-\eta), \tag{A.4}$$

$$G(0,x)=0.$$

It contains all the information encoded in the system, since the solution for any source $s(t,x)$ can be obtained through the convolution

$$u(t,x)=\int_{-\infty}^{+\infty}\int_{-\infty}^{+\infty}s(\tau,\eta)\,G(t-\tau,x-\eta)\,\mathrm{d}\tau\mathrm{d}\eta. \tag{A.5}$$

Applying the Fourier and Laplace transformations to Eq. (A.5) yields

$$u(\omega,k)=\frac{s(\omega,k)}{D(\omega,k)}, \tag{A.6}$$

where $D(\omega,k)$ is a function in the Laplace–Fourier space defined as $D(\omega,k)\equiv 1/G(\omega,k)$, with $G(\omega,k)$ being the transform of the Green's function. For the sake of simplicity, we assume a source function of the form $s(\omega,k)=f(\omega)\,g(k)$.

The state of the system, $u(t,x)$, is given by inverse transforming Eq. (A.6). We choose to perform first the inverse Fourier transform, which we denote as $F(\omega,x)$,

$$F(\omega,x)=\int_{-\infty}^{+\infty}\frac{g(k)}{D(\omega,k)}\exp(-ikx)\,\frac{\mathrm{d}k}{2\pi}, \tag{A.7}$$

and then the inverse Laplace transform

$$u(t,x)=\int_{-\infty-i\sigma}^{+\infty-i\sigma}F(\omega,x)\,f(\omega)\exp(i\omega t)\,\frac{\mathrm{d}\omega}{2\pi}. \tag{A.8}$$

The integration in Eq. (A.7) is carried out along the real k axis (Fourier contour), and the integration in Eq. (A.8) is performed in the line $\mathrm{Im}(\omega)=-\sigma$ (Laplace contour). This line is placed below all the singularities in the integrand in order to ensure that $u(t,x)$ be zero for $t<0$.

2. Response to a single-mode: Dispersion relation

If the excitation consists of a single mode, $s(t,x)\sim\exp(-ik_0x)$, then $g(k)\sim\delta(k-k_0)$. The inverse Fourier transform of Eq. (A.6) gives $F(\omega,x)\sim\exp(-ik_0x)/D(\omega,k_0)$. Assuming that $F(\omega,x)$ decays sufficiently fast, the inverse Laplace transform can be performed by summing over the poles of this expression, that is, the points in the ω complex plane where $D(\omega,k_0)=0$. Denoting ω_0 the pole with lowest imaginary part, the asymptotic behavior in time of the system will be given by $u(t,x)\sim\exp[-\omega_{0i}t+i(\omega_{0r}t-k_0x)]$, with the subscripts i and r denoting the imaginary and real part, respectively. If $\omega_{0i}<0$, then the system is unstable to excitations with wave number k_0, and the perturbation will grow without limit.

The equation $D(\omega,k)=0$ corresponds then to the dispersion relation of the system. It yields the unstable waves supported by the system, that is, the poles $\omega(k)$: $D(\omega,k)=0$ satisfying $\mathrm{Im}[\omega(k)]<0$ for a given real k.

3. Response to a localized source: Convective and absolute instabilities

Excitations are typically not single mode but rather they consist of a wave packet (integral over real k) with compact support in x, i.e., $g(k)$ has no poles and decays sufficiently fast. The main difference with respect to the response to a single mode lies in the fact that, even if some k are unstable, that does not ensure the response of the system to grow indefinitely at a fixed x position.

We can therefore distinguish between absolute and convective instabilities, as sketched in Fig. 8. In a convective instability, $u(t,x)$ remains bounded at $x=$ const., and usually tends to zero

$$\lim_{t\to\infty}|u(t,x)|=0.$$

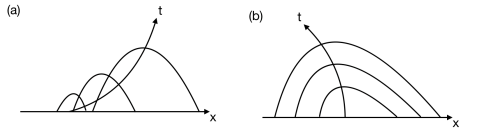

Figure 8. Sketches of (a) convective and (b) absolute instabilities. Sketch similar to Fig. 2.1 in Ref. [30].

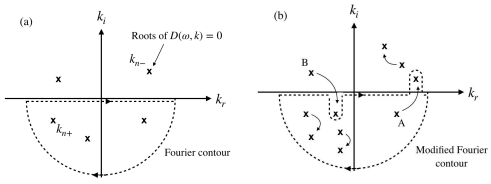

Figure 9. Fourier integration contour for $x > 0$. (a) Contour for $F(\omega, x)$. The roots are shown for a given ω, and they are grouped into k_{n+} (lower-half plane) and k_{n-} (upper-half plane). (b) Contour deformed for the analytic continuation $\tilde{F}(\omega, x)$. The position of the roots move as the imaginary ω part varies from $\omega_i = -\sigma$ to $\omega_i = 0$. Sketch similar to Figs. 2.5 and 2.9 in Ref. [30].

The initial perturbation travels or drifts as it is amplified, hence the state of the system at a fixed x position becomes amplified when the disturbance reaches it but eventually decays. Contrary to this, if a system is absolutely unstable, the perturbation grows without limit at every point x, hence

$$\lim_{t\to\infty} |u(t,x)| = \infty.$$

We apply the property of contour deformation for integration in complex domain to Eqs. (A.7) and (A.8). The Fourier contour can be closed in the lower-half k plane for $x > 0$, or in the upper-half k plane for $x < 0$, see Fig. 9(a). The function $F(\omega, x)$ can therefore be expressed as a sum of normal modes that decay away from the source. For $x > 0$, we have

$$F(\omega,x) = \sum_{k_{n+}} -\frac{ig\left[k_{n+}(\omega)\right]}{\left.\frac{\partial D(\omega,k)}{\partial k}\right|_{k=k_{n+}}} \exp\left[-ik_{n+}(\omega)\,x\right], \quad \text{(A.9)}$$

with the sum being over all roots of $D(\omega, k) = 0$ whose wave numbers lie in the lower-half k plane, k_{n+}.

Since we analyze the asymptotic response in time of the system, $t \to \infty$, it is convenient to deform the Laplace contour in Eq. (A.8) as far as possible into the upper-half ω plane. The asymptotic response will be governed by the singularity of $F(\omega, x) f(\omega)$ with lowest imaginary part. We assume that the excitation is of a sinusoidal form, hence its Laplace transform has a pole in the real axis, $f(\omega) \sim 1/(\omega - \omega_f)$, with ω_f real. From inspection of Eq. (A.9), it can be seen that the singularities of $F(\omega, x)$ correspond to values of ω for which a k_{n+} or k_{n-} mode crosses the real k axis. When this happens, the number of modes in the summation is altered, and the function $F(\omega, x)$ jumps in value. Actually, the lines of complex ω for real k satisfying $D(\omega, k) = 0$ are branch lines of the function $F(\omega, x)$. When these branch lines lay in the lower-half ω plane, the Laplace contour cannot be deformed into the real ω axis. This is the mathematical consequence of the system supporting unstable waves. It is better then to opt for another strategy, namely performing an analytical continuation of $F(\omega, x)$ through these branch lines. The analytical continuation can be done by deforming the Fourier contour in order to "follow" the roots that cross the real k axis [see Fig. 9(b)]. Depending on whether this operation can be performed, we will characterize the system as convectively or absolutely unstable.

a. *Convective instability*

If the analytical continuation can be done, the function thereby constructed, denoted $\tilde{F}(\omega, x)$, does not have these branch lines along the contours of complex ω for real k. It can be expressed as sum of modes as in Eq. (A.9), with the requirement that only the roots that have k in the lower-half k plane when $\omega_i < -\sigma$ enter in the sum. For example, in Fig. 9(b), the root A would enter in the sum but the root B would be excluded for $x > 0$. When using the analytic continuation, the Laplace contour can be deformed into a line just above the real ω axis without encountering any other singularity but the one of $f(\omega)$. The asymptotic response would therefore behave as

$$\lim_{t\to\infty} u(t,x) = \tilde{F}(\omega_f, x) \exp(i\omega_f t). \quad \text{(A.10)}$$

The space dependence far from the source is mainly given by mode A, $\tilde{F}(\omega_f, x) \sim \exp\left[k_{Ai}(\omega_f)\,x\right]$, which is an amplifying wave for $x > 0$. Similarly, mode B in Fig. 9(b) would be an amplifying wave that develops for $x < 0$. The rest of the modes are evanescent waves since they do not cross the real k axis.

The asymptotic response [Eq. (A.10)] corresponds to a convective instability where the perturbation grows exponentially as it drifts away from the source, but it remains bounded for $x =$ const. Besides, the temporal behavior of the system is given by the frequency of the external source, not by any internal frequency inherent in the system.

b. *Absolute instability*

The analytic continuation cannot always be performed. When the amplifying wave merges with an evanescent wave, the path of integration is "stuck" between both

poles and it cannot be further deformed, see Fig. 10(a). The Fourier integration must be carried out between the two merging roots, resulting in a singularity of the function $\tilde{F}(\omega, x)$ at the value $\omega = \omega_s$ for which the two roots merge. Letting k_s denote this double root, the dispersion relation can be approximated in a neighborhood around (ω_s, k_s) by

$$D(\omega, k) \simeq \left.\frac{\partial D}{\partial \omega}\right|_s (\omega - \omega_s) + \frac{1}{2}\left.\frac{\partial^2 D}{\partial k^2}\right|_s (k - k_s)^2 . \quad \text{(A.11)}$$

Notice that the merger of roots is equivalent to requiring that the dispersion relation $\omega(k) : D(\omega, k) = 0$ present a saddle point, $\mathrm{d}\omega/\mathrm{d}k = 0$.

Inserting the previous expression in the definition of $\tilde{F}(\omega, x)$, we find that, close to $\omega = \omega_s$, we have

$$\tilde{F}(\omega, x) \simeq \frac{g(k_s)}{\sqrt{2\left.\frac{\partial D}{\partial \omega}\right|_s \left.\frac{\partial^2 D}{\partial k^2}\right|_s}} \frac{\exp(-ik_s x)}{\sqrt{\omega - \omega_s}}. \quad \text{(A.12)}$$

This expression has the structure of a branch pole, and is valid for both $x > 0$ and $x < 0$. Consequently, it must be taken into account when integrating in the Laplace contour, see Fig. 10(b). The main contribution in the asymptotic response in time no longer comes from the source, but rather from the branch pole. It has the form of

$$\lim_{t\to\infty} u(t, x) = \frac{g(k_s) f(\omega_s)}{\sqrt{2\pi i \left.\frac{\partial D}{\partial \omega}\right|_s \left.\frac{\partial^2 D}{\partial k^2}\right|_s}} \frac{\exp\left[-\omega_{si} t + i(\omega_{sr} t - k_s x)\right]}{\sqrt{t}}. \quad \text{(A.13)}$$

This asymptotic response corresponds to an absolute instability if $\omega_{si} < 0$, and the perturbation grows uncontrollably everywhere in the system.

It is important to highlight that, in order to derive Eq. (A.12), the two merging roots must come from different halves of the complex k plane (upper k_{n-} and lower k_{n+}) so that the path of integration gets stuck between the two. In the words of Briggs [30], the root merging corresponds to a spatial "resonance" inherent to the system, and the structure developed by the perturbation Eq. (A.13) is independent of the excitation source. If the two merging roots come from the same half, however, the integration path would surround them and the singularities would cancel out.

c. *Comparison with other criteria*

A similar criterion for absolute instability has been derived by other authors, Refs. [29, 31, 32], where the inverse Laplace transform was applied first to Eq. (A.6), resulting in

$$G(t, k) = \int_{-\infty - i\sigma}^{+\infty - i\sigma} \frac{f(\omega)}{D(\omega, k)} \exp(i\omega t) \frac{\mathrm{d}\omega}{2\pi}. \quad \text{(A.14)}$$

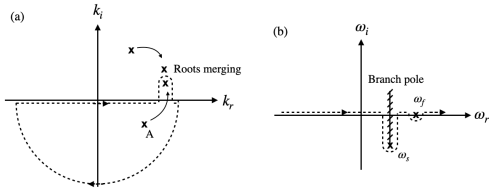

Figure 10. (a) Amplifying wave A merging with evanescent wave. (b) Branch pole in $\tilde{F}(\omega, x)$ showing an absolute instability. Sketch similar to Figs. 2.10(a) and 2.11 in Ref. [30].

Assuming that the integrand decays sufficiently fast for $|\omega| \to \infty$, we can express the previous integral as a sum over the poles of the integrand as

$$G(t, k) = \sum_\alpha \frac{i f[\omega_\alpha(k)]}{\left.\frac{\partial D(\omega, k)}{\partial \omega}\right|_{\omega_\alpha(k)}} \exp[i\omega_\alpha(k) t]. \quad \text{(A.15)}$$

Each pole $\omega_\alpha(k)$ corresponds to a sheet of the dispersion relation $D(\omega, k) = 0$. Since the integration contour $\omega = -i\sigma$ is placed below all the singularities of the integrand in Eq. (A.14), the total sum gives an entire function $G(t, k)$ in the Fourier variable k. Applying the inverse Fourier transform and commuting the integral and the summation gives, finally,

$$u(t, x) = \sum_\alpha \int_{-\infty}^{+\infty} \frac{i f[\omega_\alpha(k)] g(k)}{\left.\frac{\partial D(\omega, k)}{\partial \omega}\right|_{\omega_\alpha(k)}} \exp\{i[\omega_\alpha(k) t - kx]\} \frac{\mathrm{d}k}{2\pi}. \quad \text{(A.16)}$$

The instability criterion is derived from an independent analysis of each sheet. In the work of Dysthe [31], the Fourier contour (real k axis) is deformed wherever the imaginary part of $\omega_\alpha(k)$ is negative (unstable waves), as shown in Fig. 11. If the sheet presents a saddle point, $\mathrm{d}\omega_\alpha/\mathrm{d}k|_{k=k_s} = 0$, with a positive imaginary part $\mathrm{Im}[\omega_\alpha(k_s)] > 0$, it is possible to deform the contour as done in Fig. 11(a) so that the temporal dependence in Eq. (A.16) is a decaying exponential function. If this can be done for every sheet $\omega_\alpha(k)$, the system is not absolutely unstable, because the perturbations remain bounded for a fixed x.

However, if the imaginary part of the saddle point is negative, $\mathrm{Im}[\omega_\alpha(k_s)] < 0$, the contour can be deformed so that it passes through the saddle point by the path of steepest descent, Fig. 11(b). The main contribution to the asymptotic response in time comes from a small

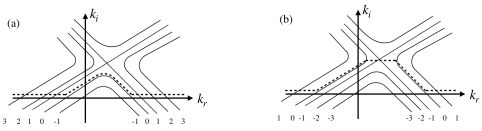

Figure 11. Deformed Fourier integration contour. The solid lines correspond to Im $\omega_\alpha(k) = \text{const}$. (a) Saddle point with positive imaginary part. (b) Saddle point with negative imaginary part. Sketch similar to Figs. 1 and 2 in Ref. [31].

neighborhood around the saddle point and, as shown in Eq. (19) in Ref. [31], it takes the same expression as Eq. (A.13). The perturbation increases exponentially in time and the system would therefore be absolutely unstable.

Although the root merging condition, required for the criterion in Briggs [30], is mathematically the same as the saddle point condition, both instability criteria are not exactly equivalent. Briggs requires additionally that the two roots come from different halves of the complex k plane. If one of the roots crosses the real k axis an even number of times, then $\partial D/\partial\omega = 0$ at some point and both criteria would disagree. The discrepancy resides in not having properly assessed the singularities of the integrand in Eq. (A.16), which precisely correspond to the branch poles of the sheet $\omega_\alpha(k)$ satisfying $\partial D/\partial\omega|_{\omega_\alpha(k)} = 0$. Assuming that the contour deformation in Fig. 11 could be performed indirectly neglected the contribution of these singularities. Although these singularities cancel out when summed to form the entire function $G(t,k)$, they must be taken into account since the derivation of this criterion is based on the analysis of each sheet separately. When these singularities are placed between the deformed contour and the real k axis, the existence of a saddle point with negative imaginary frequency does not ensure absolute instability.

Therefore, it is not only necessary for a system to be absolutely unstable that the dispersion relation admits solutions $\omega(k)$ presenting a saddle point $\mathrm{d}\omega/\mathrm{d}k|_s = 0$ with $\mathrm{Im}[\omega(k_s)] < 0$, but also that the saddle point corresponds to a merger of roots coming from different halves of the complex k plane.

4. Relation to the stability of nonuniform systems to short wavelength transversal perturbations

There is a certain resemblance between the criteria for absolute instability in uniform systems that we just derived and the stability of nonuniform systems to short-wavelength transversal perturbations.

Consider a nonuniform system whose perturbed state $\vec{q}$ is governed by the linear equation

$$\frac{\mathrm{d}\vec{q}}{\mathrm{d}x} = \mathcal{M}(x,\omega,k_y;\Pi)\cdot\vec{q}, \tag{A.17}$$

where $\mathcal{M}$ is a general matrix representing the linearized governing equations, ω and k_y are the normalized temporal frequency and the transversal wavenumber of the perturbations, respectively, and Π corresponds to the dimensionless governing parameters. A characteristic velocity u_c and length scale L_c in the streamwise x direction have been used for normalization. The stability of the system is given by the (global) dispersion relation, which corresponds to the function $\omega(k_y;\Pi)$ for which Eq. (A.17) admits nontrivial solutions $\vec{q}(x)$ that are bounded at $x \to \pm\infty$.

We consider the large wavenumber limit, $k_y \gg 1$. Taylor expanding the governing matrix $\mathcal{M}$ around $k_y^{-1} = 0$ in Eq. (A.17) yields

$$\frac{\mathrm{d}\vec{q}}{\mathrm{d}x} = \left[\sum_{j=0}^{j=\infty} k_y^{\mu-j}\mathcal{M}_j(x,\omega;\Pi)\right]\cdot\vec{q}, \tag{A.18}$$

where μ is an integer whose value depends on the particular problem to solve. Some precaution needs to be taken when assuming the order of magnitude of the temporal frequency ω and the parameters Π, which we will assume to be of order unity for now.

When the parameter μ is positive, and the leading matrix $\mathcal{M}_0$ presents no singularities in x, the solution to Eq. (A.18) may be sought by applying the Wentzel–Kramers–Brillouin (WKB) perturbation method for systems with multiple scales. A solution in the form of $\vec{q} \propto \exp\left(-ik_y^\mu \int \lambda \mathrm{d}x\right)$ is therefore attempted, where $\lambda(x)$ are the roots of the characteristic polynomial

$$D(\omega,\lambda,x;\Pi) \equiv \mathrm{Det}\left[\mathcal{M}_0(x,\omega;\Pi) + i\lambda\mathrm{I}\right] = 0. \tag{A.19}$$

The WKB approximation breaks down in the turning points $x = x_T$, where two roots of the characteristic polynomial merge and

$$\frac{\partial D}{\partial\lambda} = 0. \tag{A.20}$$

Commonly, two turning points exist and the global dispersion relation is derived from the connexion rules of merging waves[33]:

$$\int_{x_{T_1}}^{x_{T_2}} (\lambda_2 - \lambda_1)\,\mathrm{d}x = (2N+1)\,\pi, \quad \forall N = 0,1,\ldots,\infty, \tag{A.21}$$

where λ_1 and λ_2 are the two coalescent roots such that Im $(\lambda_1) < 0$ at $x \to -\infty$ and Im $(\lambda_2) > 0$ at at $x \to \infty$. This relation yields the multiple branches of the global dispersion relation. In the $k_y \to \infty$ limit, the two turning points coalesce at a point, and the main branch of the global dispersion relation, $N = 0$, is obtained from the equation[35]:

$$\frac{\partial D}{\partial x} = 0. \tag{A.22}$$

The conditions just derived are in close relation to the analysis of uniform systems. The characteristic polynomial Eq. (A.19) can be understood as the dispersion

relation of a slab around $x = \text{const.}$ treated as if it was an infinite and uniform medium. The turning point condition, Eq. (A.20), is analogous to the root merger condition required for the slab to be absolutely unstable (we recall that the merging roots λ_1 and λ_2 must come from different halves of the complex λ plane to ensure the boundedness of the solution of the nonuniform system at $x \to \pm\infty$). Finally, Eq. (A.22) states that the growth rate of the nonuniform system corresponds to the maximum growth rate amongst all the slabs $x = \text{const.}$ that are absolutely unstable. This can be proven by differentiating Eq. (A.19) and bearing into account Eq. (A.20), yielding

$$\frac{\mathrm{d}\omega}{\mathrm{d}x} = -\frac{\partial D/\partial x}{\partial D/\partial \omega} = 0, \tag{A.23}$$

where the last equality comes from Eq. (A.21).

In conclusion, the stability of a nonuniform system to short-wavelength perturbations yielding two turning points can therefore be inferred by applying the requirement for absolute instability of uniform systems to each section $x = \text{const.}$, and the growth rate of the nonuniform system would be given by the most unstable section (the one with largest growth rate).

DATA AVAILABILITY

The data that support the findings of this study are available from the corresponding author upon reasonable request.

[1] J. A. Stamper, K. Papadopoulos, R. N. Sudan, S. O. Dean, E. A. McLean, and J. M. Dawson, Phys. Rev. Lett. 26, 1012 (1971).
[2] A. Raven, O. Willi, and P. T. Rumsby, Phys. Rev. Lett. 41, 554 (1978).
[3] L. Gao, P. M. Nilson, I. V. Igumenshchev, M. G. Haines, D. H. Froula, R. Betti, and D. D. Meyerhofer, Phys. Rev. Lett. 114, 215003 (2015).
[4] P. T. Campbell, C. A. Walsh, B. K. Russell, J. P. Chittenden, A. Crilly, G. Fiksel, P. M. Nilson, A. G. R. Thomas, K. Krushelnick, and L. Willingale, Phys. Rev. Lett. 125, 145001 (2020).
[5] J. R. Rygg, F. H. Séguin, C. K. Li, J. A. Frenje, M. J.-E. Manuel, R. D. Petrasso, R. Betti, J. A. Delettrez, O. V. Gotchev, J. P. Knauer, D. D. Meyerhofer, F. J. Marshall, C. Stoeckl, and W. Theobald, Science 319, 1223 (2008).
[6] F. H. Séguin, C. K. Li, M. J.-E. Manuel, H. G. Rinderknecht, N. Sinenian, J. A. Frenje, J. R. Rygg, D. G. Hicks, R. D. Petrasso, J. Delettrez, R. Betti, F. J. Marshall, and V. A. Smalyuk, Phys. Plasmas 19, 012701 (2012).
[7] M. J.-E. Manuel, C. K. Li, F. H. Séguin, N. Sinenian, J. A. Frenje, D. T. Casey, R. D. Petrasso, J. D. Hager, R. Betti, S. X. Hu, J. Delettrez, and D. D. Meyerhofer, Phys. Plasmas 20, 056301 (2013).
[8] M. G. Haines, Can. J. Phys. 64, 912 (1986).
[9] A. Schlüter and L. Biermann, Z. Naturforschg. A 5, 237 (1950).
[10] M. J.-E. Manuel, C. K. Li, F. H. Séguin, J. Frenje, D. T. Casey, R. D. Petrasso, S. X. Hu, R. Betti, J. D. Hager, D. D. Meyerhofer, and V. A. Smalyuk, Phys. Rev. Lett. 108, 255006 (2012).
[11] L. Gao, P. M. Nilson, I. V. Igumenshchev, S. X. Hu, J. R. Davies, C. Stoeckl, M. G. Haines, D. H. Froula, R. Betti, and D. D. Meyerhofer, Phys. Rev. Lett. 109, 115001 (2012).
[12] L. Gao, P. M. Nilson, I. V. Igumenshchev, G. Fiksel, R. Yan, J. R. Davies, D. Martinez, V. Smalyuk, M. G. Haines, E. G. Blackman, D. H. Froula, R. Betti, and D. D. Meyerhofer, Phys. Rev. Lett. 110, 185003 (2013).
[13] F. García-Rubio, R. Betti, J. Sanz, and H. Aluie, Phys. Plasmas 27, 112715 (2020).
[14] F. García-Rubio, R. Betti, J. Sanz, and H. Aluie, Phys. Plasmas 28, 012103 (2021).
[15] D. A. Tidman and R. A. Shanny, Phys. Fluids 17, 1207 (1974).
[16] L. A. Bol'shov, Yu. A. Dreizin, and A. M. Dykhne, JETP Lett. 19, 168 (1974).
[17] E. S. Weibel, Phys. Rev. Lett. 2, 83 (1959).
[18] E. M. Epperlein, Plasma Phys. Control. Fusion 27, 1027 (1985).
[19] M. G. Haines, Phys. Rev. Lett. 47, 917 (1981).
[20] A. Z. Dolginov and V. A. Urpin, Sov. Phys.-JETP 50, 912 (1979).
[21] M. Ogasawara, A. Hirao, and H. Ohkubo, J. Phys. Soc. Jpn. 49, 322 (1980).
[22] A. Hirao and M. Ogasawara, J. Phys. Soc. Jpn. 50, 668 (1981).
[23] A. Fruchtman and H. R. Strauss, Phys. Fluids B 4, 1397 (1992).
[24] J. J. Bissell, C. P. Ridgers, and R. J. Kingham, Phys. Rev. Lett. 105, 175001 (2010).
[25] J. J. Bissell, R. J. Kingham, and C. P. Ridgers, Phys. Plasmas 19, 052107 (2012).
[26] D. H. Froula, J. S. Ross, B. B. Pollock, P. Davis, A. N. James, L. Divol, M. J. Edwards, A. A. Offenberger, D. Price, R. P. J. Town, G. R. Tynan, and S. H. Glenzer, Phys. Rev. Lett. 98, 135001 (2007).
[27] E. M. Lifshitz and L. P. Pitaevskifi, *Physical Kinetics*, 1st ed., Course of Theoretical Physics, Vol. 10 (Pergamon Press, Oxford, 1981).
[28] P. A. Sturrock, Phys. Rev. 112, 1488 (1958).
[29] Ya. B. Fainberg, V. Shapiro, and V. Kurilko, Sov. Phys.-Tech. Phys. 6, 458 (1961).
[30] R. J. Briggs, *Electron-Stream Interaction with Plasmas* (MIT Press, Cambridge, MA, 1964).
[31] K. B. Dysthe, Nucl. Fusion 6, 215 (1966).
[32] A. I. Akhiezer and R. V. Polovin, Sov. Phys.-Usp. 14, 278 (1971).
[33] H. L. Berk and D. Pfirsch, J. Math. Phys. 21, 2054 (1980).
[34] M. Sherlock and J. J. Bissell, Phys. Rev. Lett. 124, 055001 (2020).
[35] A. R. Piriz, J. Sanz, and L. F. Ibañez, Phys. Plasmas 4, 1117 (1997).

[36] S. I. Braginskii, in *Reviews of Plasma Physics*, edited by M. A. Leontovich (Consultants Bureau, New York, 1965).
[37] J. Delettrez, R. Epstein, M. C. Richardson, P. A. Jaanimagi, and B. L. Henke, Phys. Rev. A 36, 3926 (1987).
[38] J. Sanz, A. Liñán, M. Rodríguez, and J. R. Sanmartín, Phys. Fluids 24, 2098 (1981).
[39] R. Nora, R. Betti, K. S. Anderson, A. Shvydky, A. Bose, K. M. Woo, A. R. Christopherson, J. A. Marozas, T. J. B. Collins, P. B. Radha, S. X. Hu, R. Epstein, F. J. Marshall, R. L. McCrory, T. C. Sangster, and D. D. Meyerhofer, Phys. Plasmas 21, 056316 (2014).
[40] J. R. Davies, H. Wen, J.-Y. Ji, and E. D. Held, Phys. Plasmas 28, 012305 (2021).
[41] J. D. Sadler, C. A. Walsh, and H. Li, Phys. Rev. Lett. 126, 075001 (2021).
[42] E. M. Epperlein and M. G. Haines, Phys. Fluids 29, 1029 (1986).
[43] J.-Y. Ji and E. D. Held, Phys. Plasmas 20, 042114 (2013).
[44] I. V. Igumenshchev, A. B. Zylstra, C. K. Li, P. M. Nilson, V. N. Goncharov, and R. D. Petrasso, Phys. Plasmas 21, 062707 (2014).

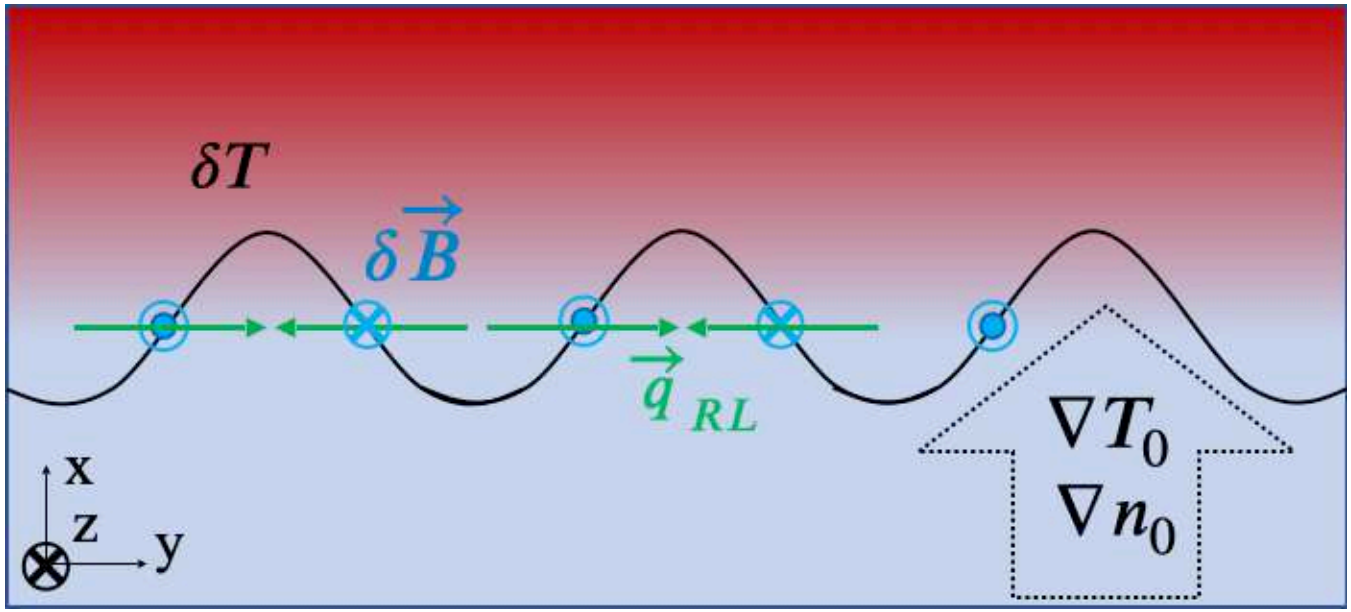

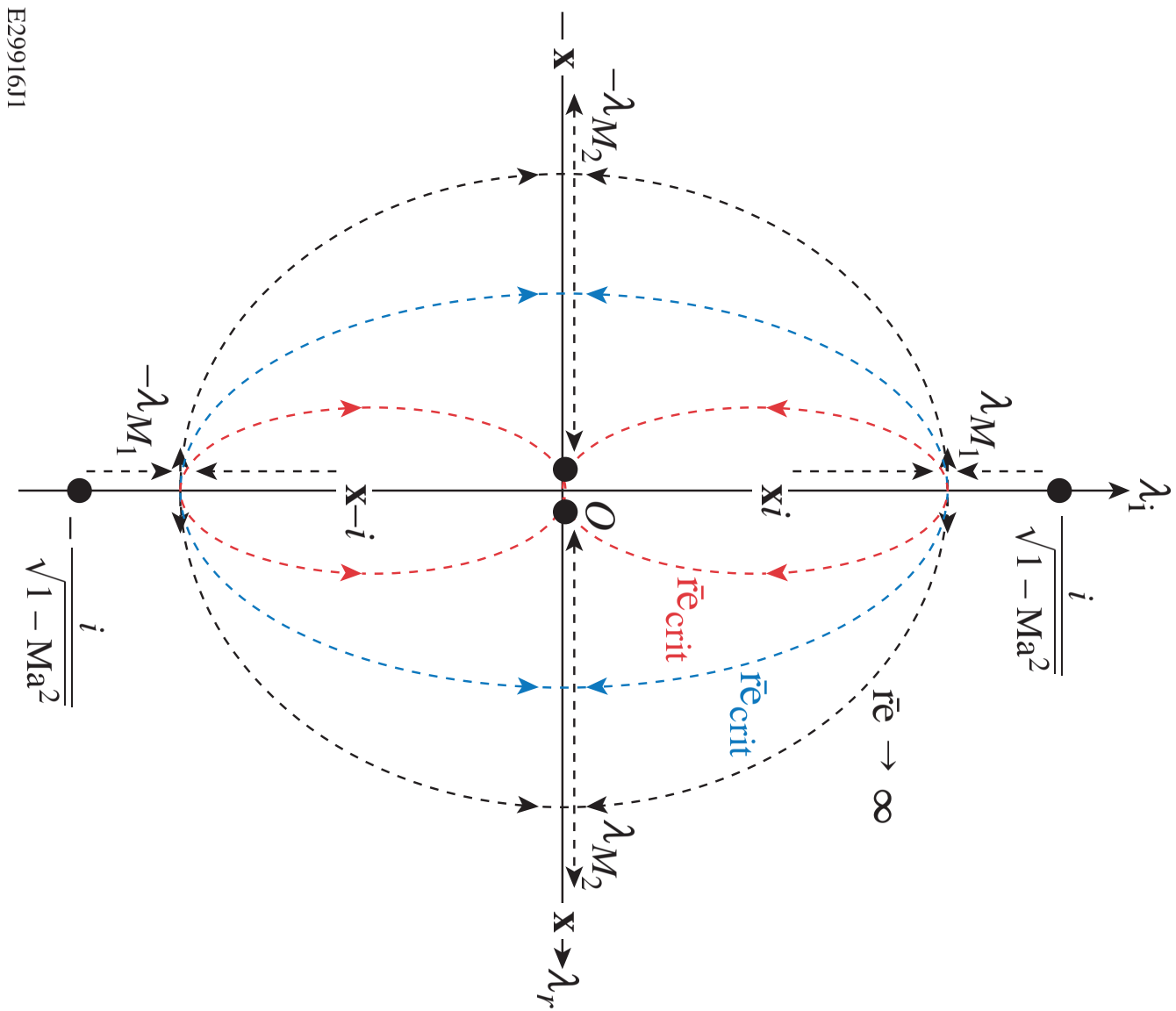

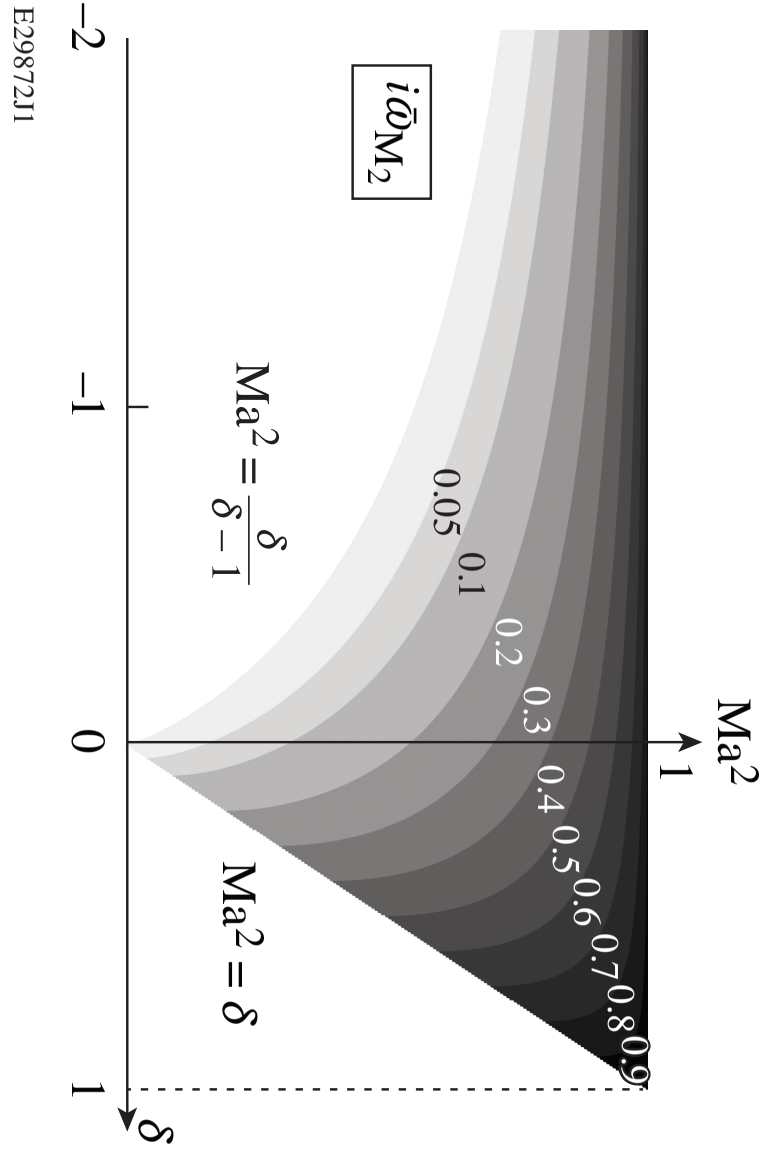

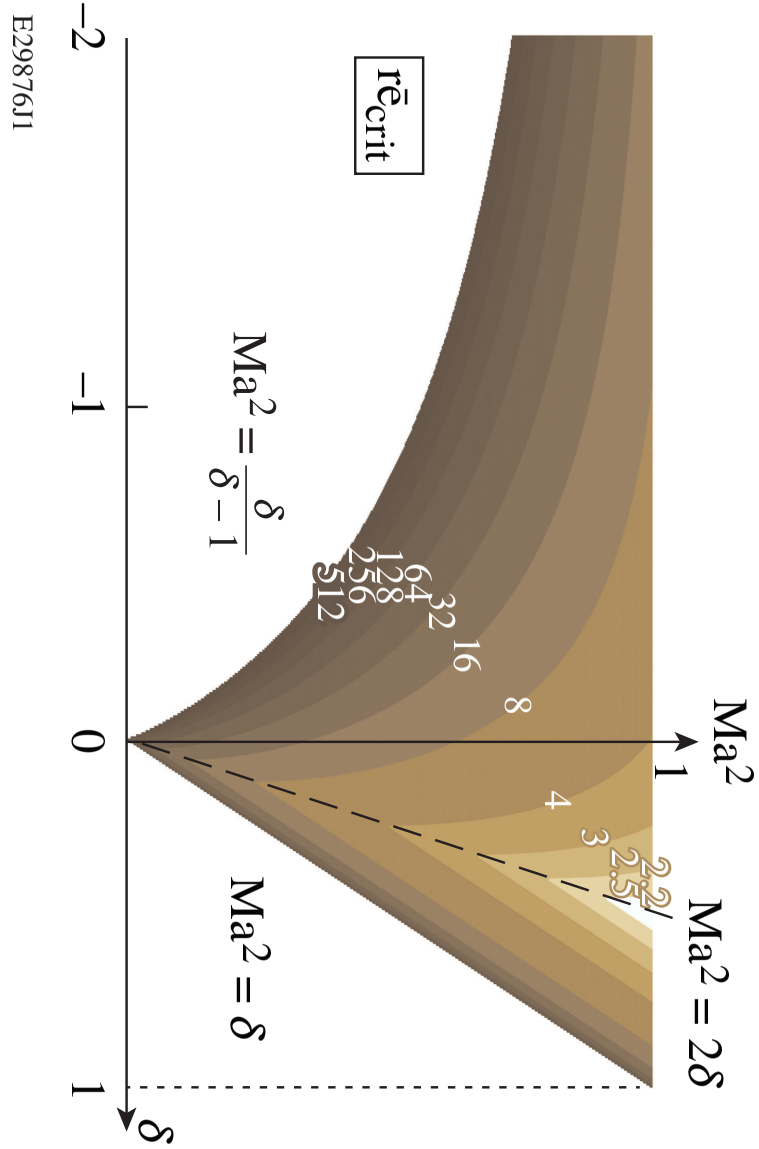

PLEASE CITE THIS ARTICLE AS DOI: 10.1063/5.0109877

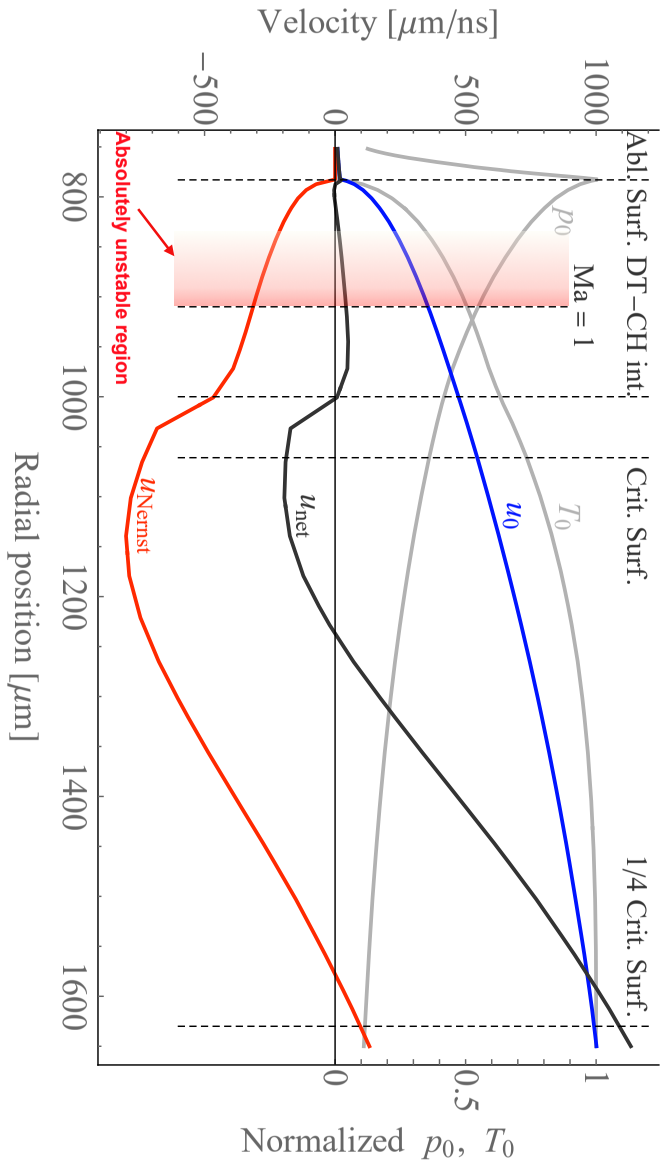

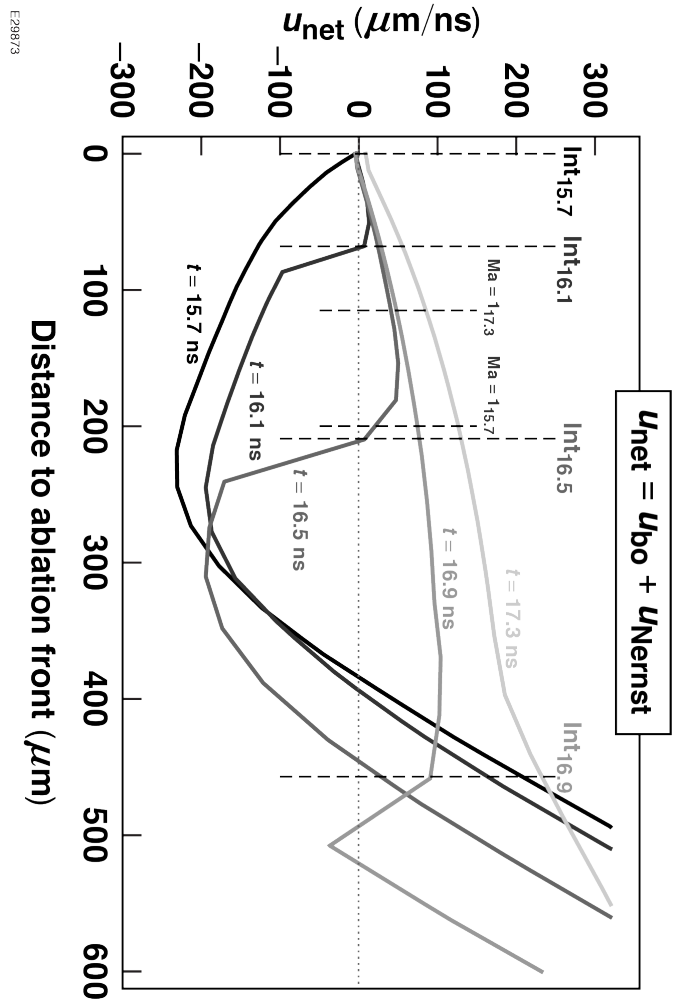

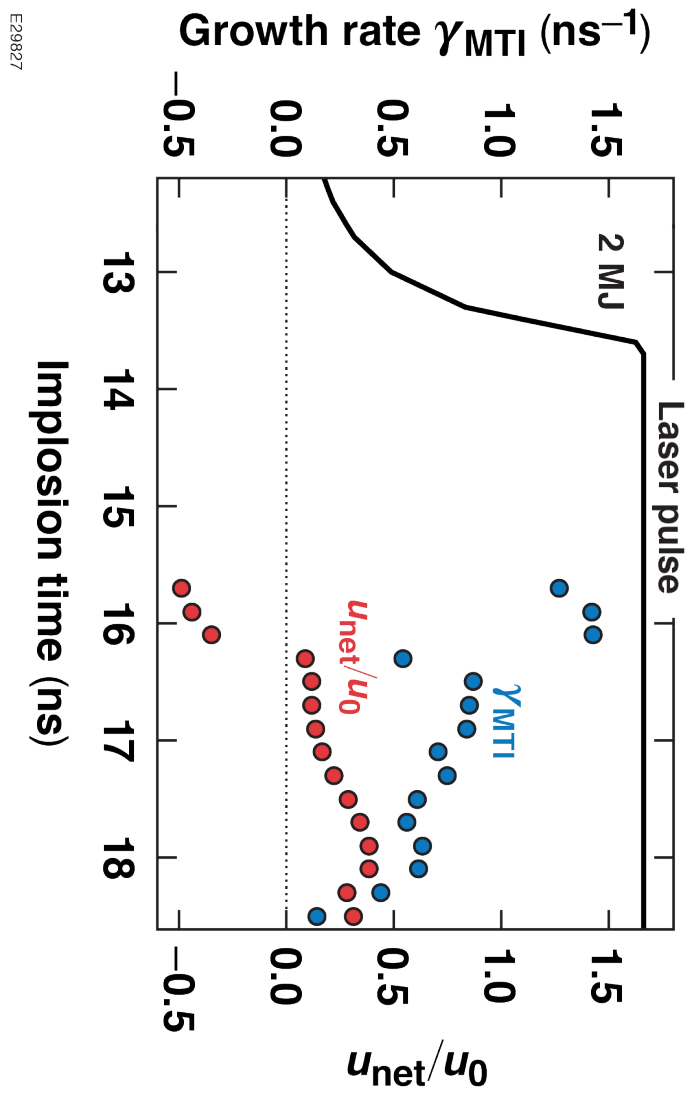

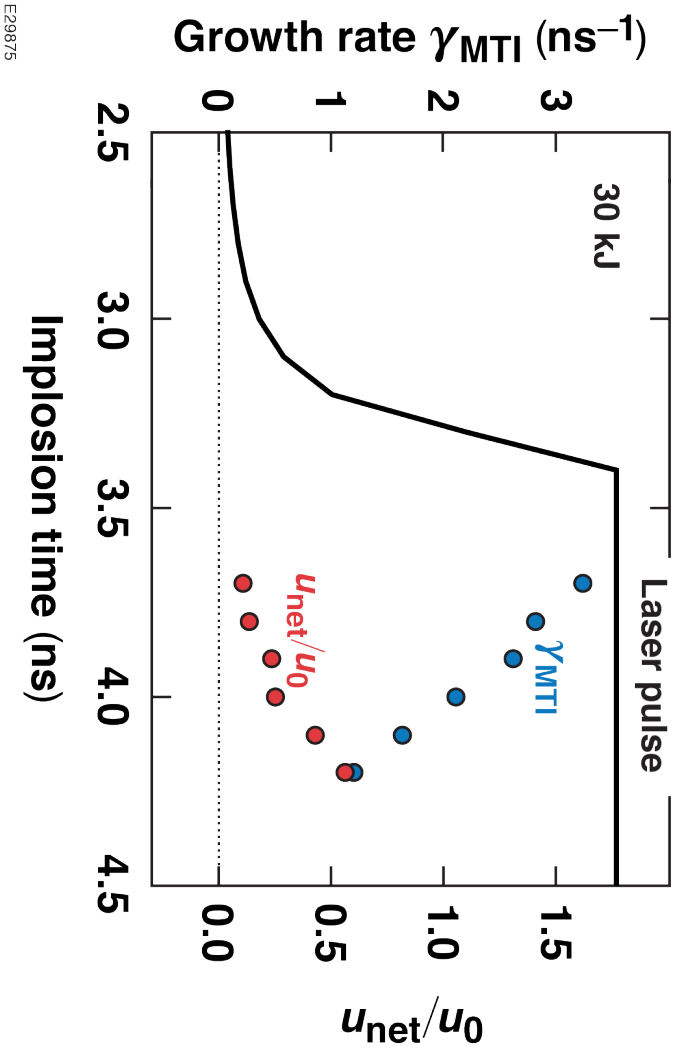

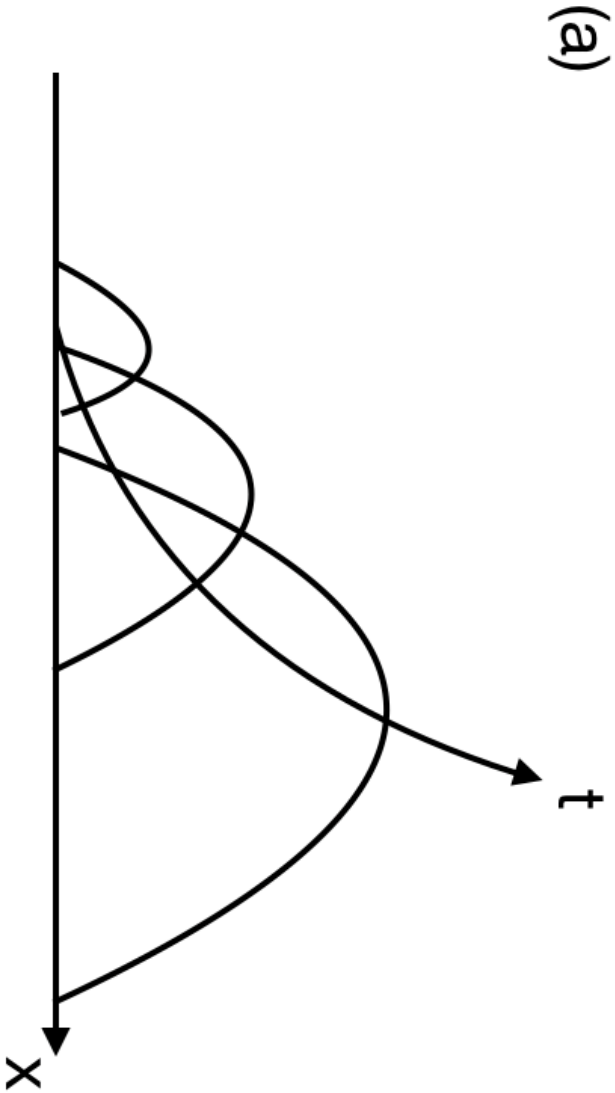

PLEASE CITE THIS ARTICLE AS DOI: 10.1063/5.0109877